ADVANCED OPTICAL MATERIALS
www.advopticalmat.de

# Multiple-Resonance-Type TADF Emitter as Sensitizer Improving the Performance of Blue Fluorescent Organic Light-Emitting Diodes

*Yaxiong Wang, Runda Guo,* Ao Ying, Kaiyuan Di, Linya Chen, Honggang Gu, Shiyuan Liu, Yalei Duan, Hanrui Su, Shaolong Gong, and Lei Wang**

**Due to the limitation of donor and acceptor group selection, the efficient thermally activated delayed fluorescence (TADF) type sensitizer used for blue organic light-emitting diodes (OLEDs) is rare. Multiple resonance (MR) type TADF emitters can easily achieve efficient blue emission. And the compounds exhibit small Stokes shift and lower absorption energy under the same emission color compared with traditional TADF, mitigating the damage of high-energy absorption of sensitizer on material stability. However, their characteristics as sensitizers have not been explored. In this work, a deep-blue MR-TADF compound (3tPAB) is selected as a sensitizer for both blue traditional fluorescence and MR-TADF OLED. Given the improved photoluminescence quantum yield and the utilization of triplet excitons, the TADF-sensitized fluorescent device using 3tPAB as sensitizer presents a maximum external quantum efficiency ($EQE_{max}$) of 14.4%, showing ≈2.4 times increase compared with the device without sensitizer. More impressively, TADF-sensitized TADF (TST) device using 3tPAB as sensitizer and MR-TADF compound PhDMAC-BN as emitter exhibits $EQE_{max}$ of 33.9%. And in TST device, efficient Förster energy transfer is demonstrated, thus, the device can maintain high color purity. The work first demonstrates the feasibility of MR-TADF as a sensitizer and provides a new strategy for developing high-performance blue OLED with high color purity.**

## 1. Introduction

Organic light-emitting diodes (OLEDs) have attracted a growing trend of attention due to their great application potential in flat-panel displays, solid-state lighting, and flexible wearable electronics.[1] For ultra-high-definition displays presented in International Telecommunication Union (ITU) Recommendation BT 2020 standard, the emitter is required to be high color purity with narrow full width at half-maximum (FWHM).[2] Compared with phosphorescent complexes emitter, metal-free fluorescence emitter exhibits low cost, environmental-friendly, and multiple structural modifiability.[3] Importantly, the polycyclic aromatic framework with the non-bonding molecular orbitals endowed organic fluorescent emitter with narrowband emission.[4] As we know, the commercial performance of blue OLEDs still lags behind that of red and green OLEDs.[5] Therefore, the research based on efficient blue organic fluorescent material with narrowband emission has become a hot subject at present.

There are two main approaches to prepare high-performance blue OLED with high color purity. One is developing blue emitter with narrowband emission, like traditional fluorescent emitter or multiple resonance (MR) type emitter.[6] The other one is developing blue thermally activated delayed fluorescence (TADF) sensitizer, and combining the device engineering to further improve device performance.[7] Although most of the current research focuses on the former, it should be emphasized that the latter is equally important for improving device performance, especially for efficiency, efficiency roll-off, and operating lifetime. For instance, by using TADF type molecule 10-phenyl-10*H*,10″*H*-spiro[acridine-9,9″-anthracen]-10′-one (ACRSA) as sensitizer, the external quantum efficiency (EQE) of traditional blue fluorescence device based on TBPe as emitter can be increased from ≈1% to 13.4%.[8] And the EQE of the corresponding device was further improved to 24.0% by further designing more advanced TADF sensitizer.[1c,7a,b,9] Similarly, in 2019, Lee et al. also employed the TADF molecule DMAC-DPS as sensitizer to improve the device performance of the MR-TADF emitter (t-DABNA).[10] After the addition of DMAC-DPS

Y. Wang, R. Guo, K. Di, Y. Duan, H. Su, L. Wang
Wuhan National Laboratory for Optoelectronics
Huazhong University of Science and Technology
Wuhan 430074, People's Republic of China
E-mail: runda_guo@hust.edu.cn; wanglei@mail.hust.edu.cn
A. Ying, S. Gong
Hubei Key Lab on Organic and Polymeric Optoelectronic
Materials Department of Chemistry
Wuhan University
Wuhan 430072, People's Republic of China
L. Chen
School of Optical and Electronic Information
Huazhong University of Science and Technology
Wuhan 430074, People's Republic of China
H. Gu, S. Liu
State Key Laboratory of Digital Manufacturing Equipment and Technology
Huazhong University of Science and Technology
Wuhan 430074, People's Republic of China
The ORCID identification number(s) for the author(s) of this article can be found under https://doi.org/10.1002/adom.202202034.

**DOI: 10.1002/adom.202202034**

sensitizer, the EQE of the device was enhanced from 25.1% to 31.4%, and the efficiency roll-off was dramatically suppressed. More importantly, the device lifetime was also improved by more than 10 times (LT50 close to 35 h at 100 cd $m^{-2}$). Subsequently, Duan et al. substituted p4TCzPhBN with a more stable structure for the DMAC-DPS.[7d] The device lifetime was further improved to 60 h up to 80% of the initial luminance of 1000 cd $m^{-2}$. These works clearly demonstrate that the design of advanced TADF sensitizer is of great significance to the improvement of blue device performance. However, due to the limitation of donor and acceptor (D and A) group selection, only few blue TADF emitters were used as sensitizers for blue OLED.[7c,11] Therefore, it is highly desired to develop new-type efficient TADF sensitizers for the improvement of blue OLED with high color purity.

In 2016, Hatakeyama and coworkers reported a novel class of MR-type TADF emitters.[12] The localization of the highest occupied molecular orbitals (HOMO) and the lowest unoccupied molecular orbitals (LUMO) on different atoms as well as a rigid fusion framework endowed this material with narrow FWHM and high photoluminescence quantum yield (PLQY). Moreover, efficient blue emission can be easily achieved by reasonably controlling the conjugation degree of molecules and the arrangement position of electron-donating and -accepting atoms.[2a,4,13] Remarkably, recent studies have revealed the rate of triplet-to-singlet reverse intersystem crossing can reach $1.8 \times 10^8$ $s^{-1}$ by heavy-atom effect.[14] But until now, this type of material is only used as emitter, their characteristics as sensitizer have not been explored.

In this work, we employed a deep-blue MR-TADF material (3tPAB) with weak concentration dependence as sensitizer for blue traditional fluorescence emitter (DtPAPy) and a new synthesized MR-TADF emitter (PhDMAC-BN).[15] The deep-blue emission of 3tPAB ensured a large spectral overlap between the photoluminescence (PL) spectra of the sensitizer and the absorption of the emitter, which further induced the occurrence of Förster energy transfer (FET). Due to enhanced PLQY and the utilization of triplet excitons, the TADF-sensitized fluorescent (TSF) device based on DtPAPy as emitter achieved maximum external quantum efficiency ($EQE_{max}$) of 14.4%, The quantum efficiency was improved by ≈2.4 times compared with the conventional DtPAPy fluorescent device. In addition, MR-TADF type sensitizers also showed great potential in TADF-sensitized TADF (TST) devices. The TST device using 3tPAB as sensitizer and PhDMAC-BN as emitter exhibited $EQE_{max}$ of 33.9%, which was significantly higher than 27.2% for those devices without sensitizer. The work demonstrated the feasibility of MR-TADF material as sensitizer, opening a new strategy for the improvement of blue OLED with high color purity.

## 2. Results and Discussion

### 2.1. The Selection and Design of Sensitizer and Emitter

In TADF sensitization systems, effective FET can relieve excitons quenching and improve device performance, especially for the traditional fluorescent emitter. Therefore, the sensitizer and emitter should be carefully chosen for effective FET. According to the Förster energy transfer rate ($k_{FET}$) equation:[16]

$$k_{FET} = \frac{1}{\tau_D} \times \frac{1}{r^6} \times \frac{9000(\ln 10)\kappa_p^2 Q_D I}{N_A 128\pi^5 n_D^4} \quad (1)$$

$k_F$ is greatly influenced by $\tau_D$, $r$, $Q_D$, and $I$, where $\tau_D$ is the excited-state radiative lifetime of the sensitizer, $r$ is the separation distance between the sensitizer and emitter pair, $\kappa_p$ is a parameter about the relative orientation of the sensitizer and emitter dipoles, $Q_D$ is the PLQY of sensitizer, $I$ is the spectral overlap integral between the emission of sensitizer and the absorption of the emitter, $N_A$ is Avogadro's number, $n_D$ is the refractive index of the medium. Accordingly, decreasing $\tau_D$ and $r$, and increasing $Q_D$ and $I$ are greatly important to achieve effective energy transfer. The low $r$ can be achieved by increasing the doping concentration of the sensitizer or emitter. However, most TADF materials show reduced PLQY at a high doping concentration due to a strong concentration-induced quenching effect. Therefore, to maintain the luminescence performance of the emitter, the low doping concentration of the emitter and the high doping concentration of the sensitizer are usually adopted to ensure effective energy transfer.[5e] This indicates the sensitizer should be weak concentration dependence to keep a high PLQY. Besides, for blue OLED, the TADF sensitizer also needs to exhibit at least pure blue or even deep-blue emission to acquire high $I$ relative to absorption of the blue emitter.

Based on the above discussion, 3tPAB was selected, a MR-TADF emitter, as a new-type deep-blue TADF sensitizer. Due to the cladding of peripheral *tert*-butyl groups, 3tPAB showed weak concentration dependence. For example, at a low doping concentration of 5 wt.%, the PLQY of 3tPAB doped in the PPF host was as high as 85.4%, and EQE of the corresponding electroluminescent device was 25.8% (Figure S1 and Table S1, Supporting Information). At a higher doping concentration of 20 wt.%, 3tPAB still maintained excellent luminescence performance with the PLQY of 78.3%, EQE of 20.3%, and satisfactory deep-blue emission. Specifically, compared with traditional TADF sensitizer with D-A type structure, 3tPAB exhibited small Stokes shift value due to the rigid molecular structure and MR distribution characteristic. This means MR-TADF sensitizer will show lower absorption energy under the same emission color, which can mitigate the damaging of high-energy absorption of sensitizer on material stability. The similar molecular orbital levels of B/N-based MR-TADF compound can also suppress the carrier trapping on emitter when MR-TADF compound was served as TADF sensitizer for MR-TADF emitter. Moreover, the presence of *tert*-butyl in 3tPAB effectively inhibited Dexter energy transfer (DET) when it served as a sensitizer for the traditional fluorescent emitter, thus improving device efficiency.

To clarify the potential of MR-TADF 3tPAB as a sensitizer, we selected two blue luminescent materials (DtPAPy and PhDMAC-BN) with similar emission colors as the emitter. The molecular structure was depicted in **Figure 1**. DtPAPy was a traditional fluorescence emitter, which was reported in previous literature,[15b] while PhDMAC-BN was designed as a new MR-TADF emitter. The selection and design of the material were

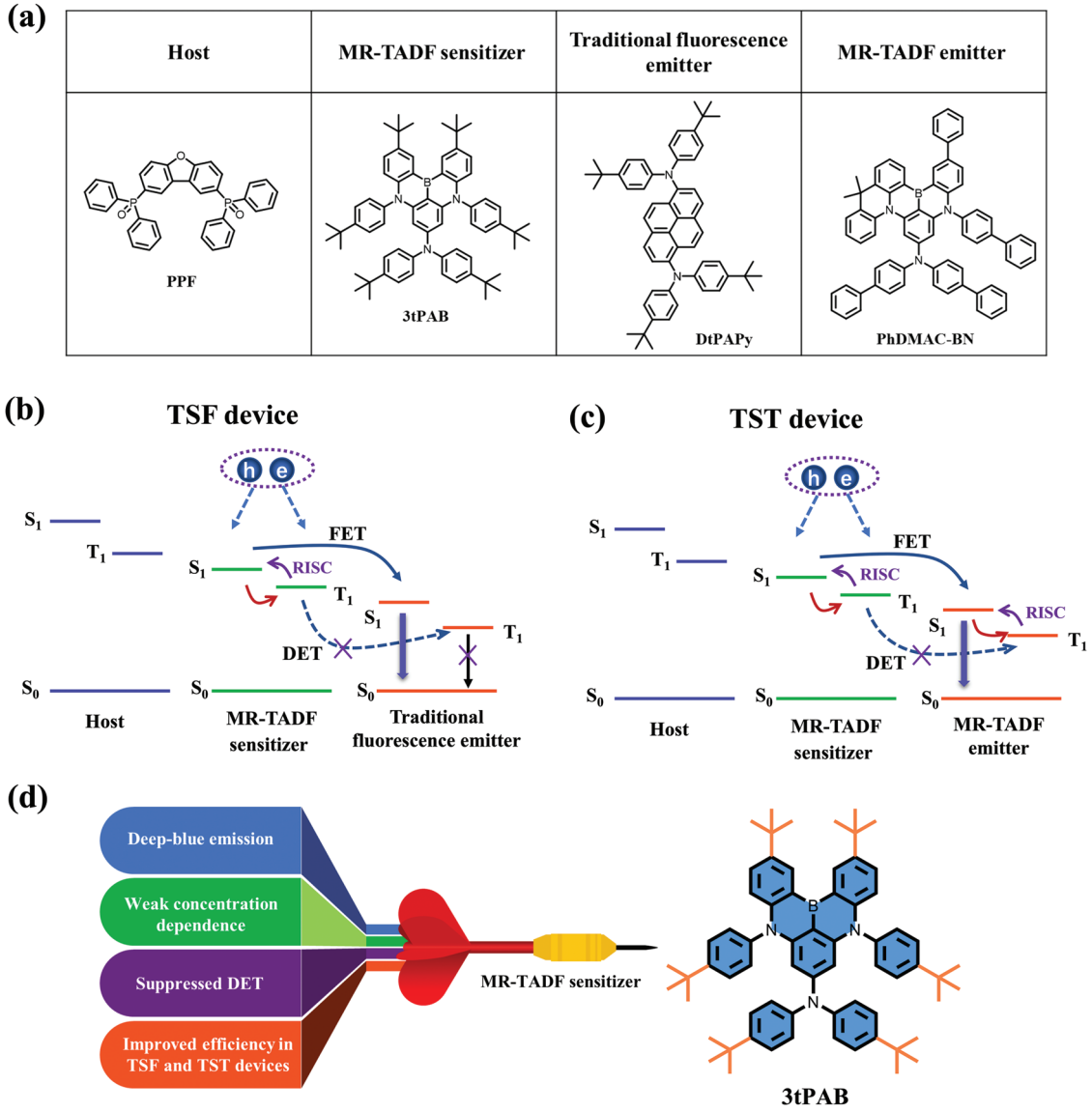


**Figure 1.** a) Chemical structures of PPF, 3tPAB, DtPAPy, and PhDMAC-BN. Schematic of the energy transfer mechanisms for the b) TSF device and c) TST device. d) The properties of the selected MR-TADF sensitizer.

based on the following considerations. In DtPAPy, the *tert*-butyl group would further spatially modulate the sensitizer-to-emitter distance and suppress their energy exchange of triplet excitons via DET. In PhDMAC-BN, diphenyl ring hanging on MR core skeleton will not only regulate DET like *tert*-butyl group but also adjust the emission color and efficiency of the compound. Compared to traditional fluorescence emitter, the delayed fluorescence characteristics and narrow-band emission of PhDMAC-BN will be beneficial for further improving the efficiency and color purity of the electroluminescent devices.

### 2.2. Physical and Chemical Properties of MR-TADF Emitter

To judge the luminescence ability of new synthesized compound, the physical and chemical properties of PhDMAC-BN were first investigated. The synthetic route of PhDMAC-BN was listed in Scheme S1, Supporting Information. The chemical structure of the target product was confirmed by nuclear magnetic resonance (NMR) spectroscopy ($^{1}$H NMR and $^{13}$C NMR) and mass spectrometry. Frontier orbitals distribution characteristics, thermal properties, electrochemical properties, and photophysical properties of the new synthesized MR-TADF emitter were investigated to reveal the structure-property relationship of the new compound. Figure S2, Supporting Information, presented the frontier molecular orbital distribution of PhDMAC-BN. HOMO was principally localized on the nitrogen atom and the ortho/para-positioned carbon atoms, while LUMO was mainly distributed on the boron atom and their ortho/para-positioned carbon atoms and slightly extended to diphenylamine substituent. This feature obeyed the multiple resonance effect, indicating the narrowband emission

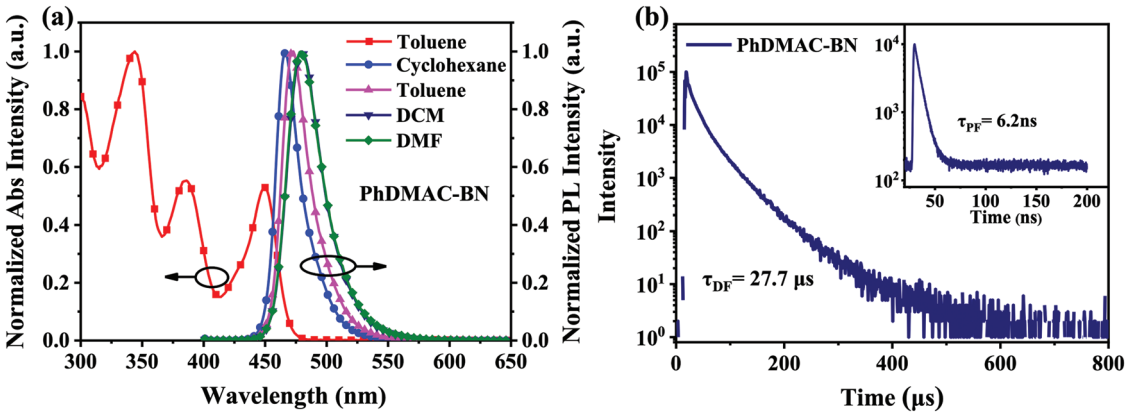


**Figure 2.** a) The UV-vis absorption and PL spectra of PhDAMC-BN. b) The transient PL spectra of PPF: 5wt% PhDAMC-BN film.

characteristics of PhDMAC-BN. The $E_g$ with 3.45 eV and high oscillator strengths $f(S_0 - S_1)$ value with 0.238 were calculated, respectively, which anticipated PhDMAC-BN was a blue emitter with efficient radiative decay.

The decomposition temperatures ($T_d$) at 5% weight reduction and the glass-transition temperature ($T_g$) of PhDMAC-BN were measured by thermogravimetric analysis (TGA) and differential scanning calorimetry (DSC), respectively. The observed $T_d$ and $T_g$ values were 414 °C and 195 °C (Figure S3, Supporting Information), respectively, demonstrating the excellent thermal and morphological stability of PhDMAC-BN. The HOMO energy level of PhDMAC-BN was measured by Cyclic voltammetry (CV) measurement (Figure S4, Supporting Information). From the onset of the first oxidation wave, the calculated HOMO level was −5.20 eV by using bis(cyclopentadienyl)iron (ferrocene) as the standard reference. And the LUMO energy level was estimated to be −2.56 eV according to the HOMO and optical bandgap ($E_{opt}^g$).

The UV-Visible absorption and PL spectra were measured to investigate the basic photophysical properties of PhDMAC-BN. A strong absorption band with a maximum of 449 nm was observed in toluene solution (**Figure 2**a), which primarily originated from the MR-induced short-range charge transfer transitions. The $E_{opt}^g$ of PhDMAC-BN was calculated to be 2.64 eV from the UV-vis absorption edges. PhDMAC-BN exhibited pure-blue emission with a peak wavelength of 473 nm and FHWM of 27 nm in toluene solution. The corresponding Stokes shift was 24 nm. Such small FHWM and Stokes shift values revealed the suppressed geometry relaxation, suggesting the highly rigid conjugated framework of PhDMAC-BN. As the solvent was changed from cyclohexane to *N*, *N*-dimethylformamide, the emission of PhDMAC-BN was redshifted by 13 nm (Table S2, Supporting Information), which verified the short-range charge transfer characteristic of the compound. The energy difference value between singlet and triplet energies ($\Delta E_{ST}$) was calculated to be 0.14 eV from the peak wavelength of low-temperature (77 K) fluorescence and phosphorescence spectrum spectra (Figure S5, Supporting Information). Such a small $\Delta E_{ST}$ value was favorable for TADF emission by the up-conversion from triplet exciton to singlet exciton.

The photophysical parameters of PhDMAC-BN doped in PPF with the doping concentration of 5wt% were subsequently collected. In the doped film state, PhDMAC-BN showed sky-blue emission with a peak wavelength of 483 nm and FWHM of 34 nm (Figure S12, Supporting Information), respectively. Compared with PL spectra in toluene solution, the emission wavelength and FWHM values were red-shifted and broadened, respectively. This can be attributed to the increased polarity introduced by the host and the $\pi$-$\pi$ interaction with the host. The absolute PLQY of PhDMAC-BN in the oxygen-free doped film was subsequently tested, which was as high as 84.6%. In addition, the transient PL spectrum of the doped film was also measured to evaluate the TADF properties of PhDMAC-BN. As presented in Figure 2b and **Table 1**, the prompt fluorescence lifetime ($\tau_{PF}$) and delayed lifetime ($\tau_{DF}$) were 6.2 ns and 27.7 μs, respectively. Based on the above parameters, The rate constants for fluorescence ($k_F$), internal conversion ($k_{IC}$), intersystem crossing ($k_{ISC}$), and reverse intersystem crossing ($k_{RISC}$) of PhDMAC-BN were calculated using the reported method,[17] as summarized in Table S3, Supporting Information. The high $k_F$ of $9.98 \times 10^7$ $s^{-1}$ and $k_{RISC}$ of $5.04 \times 10^4$ $s^{-1}$ indicated the great potential of PhDMAC-BN as the emitter.

**Table 1.** Photophysical, electrochemical, and thermal analysis data of PhDMAC-BN.

| Compound | $T_g/T_d$[a)] [°C] | $\lambda_{abs}$[b)] [nm] solution | $\lambda_{em}$ [nm] solution[b)]/film[c)] | HOMO[d)]/LUMO[e)] [eV] | $E_S/E_T$[f)] [eV] | $\Phi$[g)] [%] | $\tau_{PF}$[h)] [ns] | $\tau_{DF}$[h)] [μs] | FWHM[i)] [nm] |
|---|---|---|---|---|---|---|---|---|---|
| PhDMAC-BN | 195/414 | 449 | 473/483 | −5.20/−2.56 | 2.66/2.52 | 86.4 | 6.2 | 27.7 | 27/34 |

[a)] $T_d$ was measured by TGA (corresponding to 5% weight loss) and $T_g$ was measured by DSC; [b)]The peak wavelength of the lowest-energy absorption band and the peak wavelength of the PL spectrum in toluene; [c)]The PL peak wavelength of 5 wt.% emitter: PPF film; [d)]HOMO was estimated from the CV; [e)]LUMO = HOMO + $E_{opt}^g$; [f)]Calculated from the peak wavelength of fluorescence (Fl, 77 K) and the phosphorescence (Phos, 77 K) spectra in toluene; [g)]Absolute photoluminescence quantum yields in PPF film (5 wt.%); [h)]Lifetime calculated from fluorescence decay and lifetime calculated from delayed fluorescence in the doped film of the emitter in PPF (5 wt.%); [i)]Full width at half maximum in toluene and 5 wt.% emitter: PPF film.

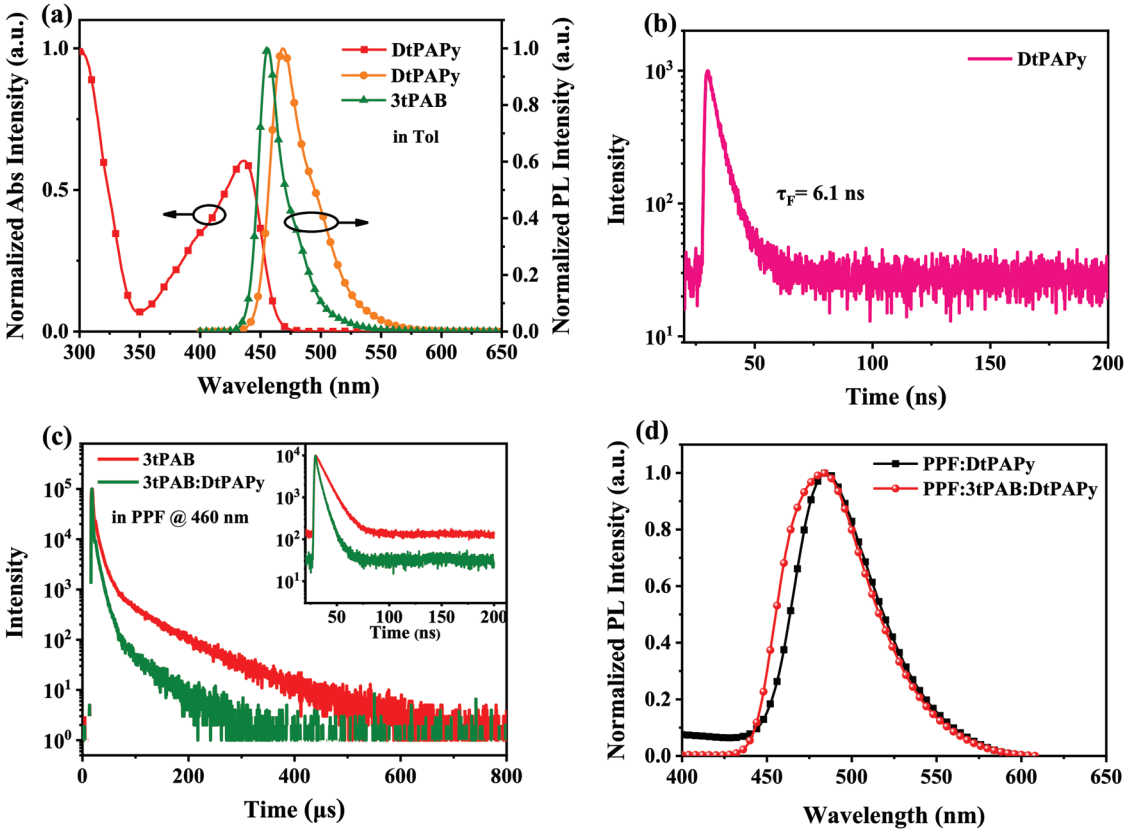


**Figure 3.** a) The UV-vis absorption and PL spectra of DtPAPy, and PL spectra of 3tPAB in toluene ($1.0 \times 10^{-5}$ M). b) The transient PL spectra for PPF: 0.5wt.% DtPAPy film. c) The transient PL spectra for PPF: 20 wt.% 3tPAB and PPF: 20 wt.% 3tPAB: 0.5 wt.% DtPAPy films. d) PL spectra of PPF: 0.5 wt.% DtPAPy and PPF: 20 wt.% 3tPAB: 0.5 wt.% DtPAPy films.

### 2.3. Performances of TSF Device

To prove the potential of MR-TADF 3tPAB as a sensitizer, traditional fluorescence material, DtPAPy, was first employed as the emitter. The steady-state PL spectra of 3tPAB emitters and absorption spectra of DtPAPy in toluene were measured to determine the possibility of FET. As shown in **Figure 3**a, an effective spectral overlap between the PL of 3tPAB and the absorption of DtPAPy was observed, demonstrating FET can occur from 3tPAB to DtPAPy. Further, the corresponding non-sensitized and TADF-sensitized OLEDs were prepared. The device structures were ITO/ $MoO_3$ (10 nm)/ TAPC (60 nm)/ mCP (10 nm)/ EML (20 nm)/ PPF (10 nm)/ TmPyPB (30 nm)/ LiF (1 nm)/ Al (100 nm). The emitting layer (EML) were PPF: *x* wt.% DtPAPy (*x* = 0.5, 1, 3) and PPF: 20 wt.% 3tPAB: *x* wt.% DtPAPy (*x* = 0.5, 1, 3) for non-sensitized and TADF-sensitized device, respectively. Here, $MoO_3$ and LiF served as hole and electron injection layers, respectively. 1,1-bis[(di-4-tolylamino)phenyl]cyclohexane (TAPC) and 1,3,5-tri(m-pyrid-3-ylphenyl)benzene (TmPyPB) were used as hole- and electron-transporting layers, respectively. 1,3-di(9H-carbazol-9-yl)benzene (mCP) was employed as exciton blocking layer. PPF served as host and exciton blocking layer. As depicted in Figures S7, S8, and Table S4, Supporting Information, the EL performance was improved greatly after the addition of sensitizer 3tPAB. As the doping concentration of DtPAPy varied from 0.5 wt.% to 3 wt.%, the $EQE_{max}$ of the non-sensitized device reduced from 6.1% to 5.5% while the $EQE_{max}$ of the TADF-sensitized device decreased from 14.4% to 8.2%. Since the guest molecule DtPAPy can not utilize the triplet excitons effectively, with the increase of doping concentration, part of the carriers recombined on the guest material, leading to the decrease of exciton utilization in the device. Therefore, the TADF-sensitized device exhibited significantly reduced efficiency with increasing doping concentration. Nevertheless, remarkably, the $EQE_{max}$ of the TADF-sensitized device was ≈2.4 times higher than the non-sensitized device at 0.5 wt% doping concentration (**Figure 4**, and **Table 2**), revealing the great potential of 3tPAB as TADF sensitizer.

To explore the origin of the superior EL performance of the 3tPAB-sensitized device, transient PL decay curves of 20 wt.% of 3tPAB with and without 0.5 wt.% of DtPAPy in PPF film were measured. As illustrated in Figure 3c, the ratio of the delayed part and the lifetime of 3tPAB were reduced after the addition of DtPAPy, suggesting energy transfer from 3tPAB to DtPAPy. The reason was the addition of DtPAPy provided an additional singlet relaxation path of the sensitizer, thus leading to a shorter decay time. Furthermore, the PLQY of the doped film was improved from 64.5% of PPF: 0.5 wt.% DtPAPy to 82.8% of PPF: 20wt.% 3tPAB: 0.5 wt.% DtPAPy. Hence, the utilization of triplet excitons and the improvement of PLQY were the reason for boosted performance of the

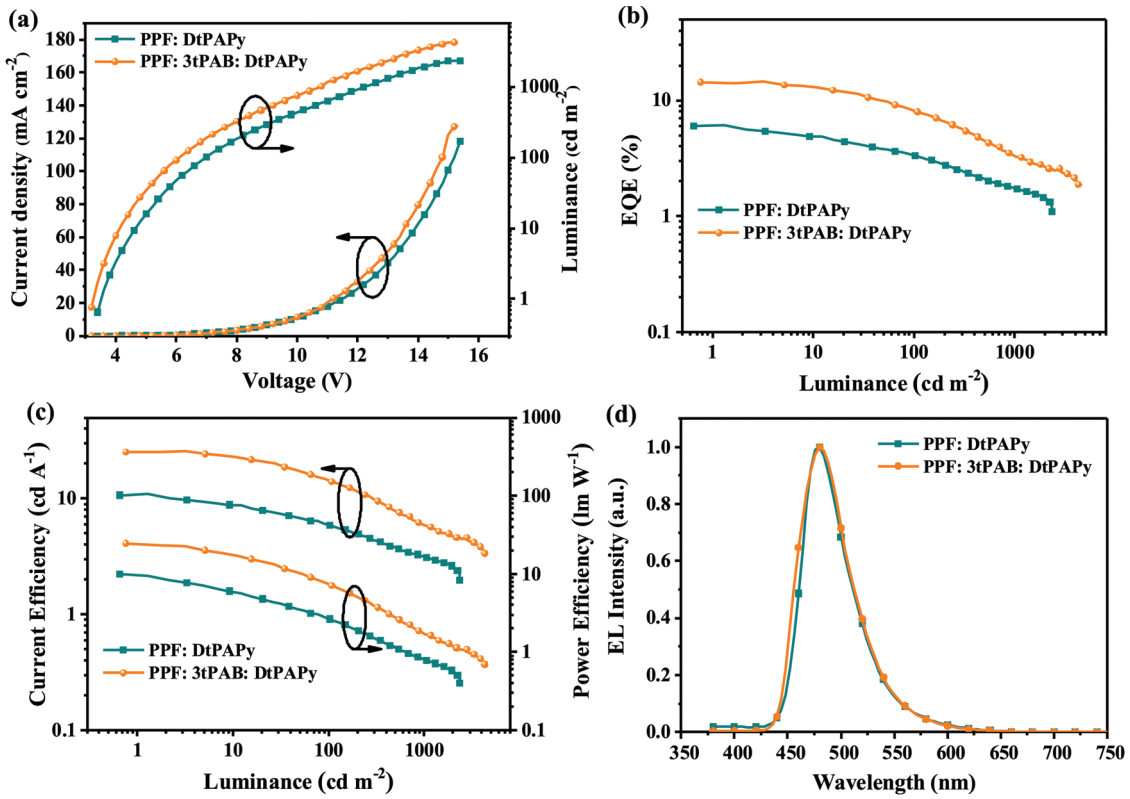


**Figure 4.** EL characteristics of the DtPAPy with 0.5 wt.% doping concentration: a) Current density-voltage-brightness (*J–V–B*) characteristics. b) EQE-brightness curves. c) current efficiency-brightness-power efficiency curves. d) normalized EL spectra at 6 V.

3tPAB-sensitized device. Nonetheless, the broadened PL spectrum and EL spectrum of sensitized films relative to that of non-sensitized films were observed (Figure 3d and Figure 4d), indicating the energy transfer was incomplete in the 3tPAB-sensitized device. This also implied the performance of the TSF device could be further improved if a more suitable emitter was selected.

### 2.4. Performances of TST Device

Given good photophysical characteristics of PhDMAC-BN, the simple doped OLEDs with device structures of ITO/ $MoO_3$ (10 nm)/ TAPC (60 nm)/ mCP (10 nm)/ PPF: xwt% PhDMAC-BN (20 nm, $x$ = 1, 3, 5, 8)/ PPF (10 nm)/ TmPyPB (30 nm)/ LiF (1 nm)/ Al (100 nm) were fabricated to explore its intrinsic luminescence properties. As presented in **Figure 5**, Figure S10, Supporting Information, and **Table 3**, at an optimal doping concentration of 5wt%, the PhDMAC-BN-based device exhibited sky-blue emission with peak wavelength of 480 nm, FWHM of 34 nm, and CIE coordinates of (0.105, 0.264), respectively. Compared with their doped film spectra, the little difference demonstrated the EL emission originated from the emitter. Simultaneously, the maximum current efficiency ($CE_{max}$)/power efficiency ($PE_{max}$)/$EQE_{max}$ also achieved 41.5 cd $A^{-1}$/39.2 lm $W^{-1}$/27.2%. To understand such high efficiency, the horizontal emitting dipole orientation ratio (Θ//) was measured, which was as high as 96% (Figure S13, Supporting Information). And combined with optical physical properties analysis, the high device efficiency can attribute to the high PLQY, satisfactory TADF property, and high Θ// of PhDMAC-BN. This demonstrated that PhDMAC-BN was an excellent MR-TADF emitter.

The effect of sensitizer 3tPAB on the performance of MR-TADF emitter PhDMAC-BN was further explored. A large spectral overlapping between the absorption spectra of

**Table 2.** The EL performances of DtPAPy with 0.5 wt.% doping concentration.

| Compound | $V_{on}$[a)] [V] | $L_{max}$[b)] [cd $m^{-2}$] | $CE_{max}$[b)] [cd $A^{-1}$] | $PE_{max}$[b)] [lm $W^{-1}$] | $EQE_{max}$[b)] [%] | $\lambda_{EL}$[c)] /FWHM[c)] [nm] | CIE[d)] [x, y] |
|---|---|---|---|---|---|---|---|
| DtPAPy | 3.5 | 2348 | 11.0/5.9/3.2 | 9.9/2.6/0.8 | 6.1/3.3/1.7 | 480/51 | (0.139, 0.289) |
| DtPAPy (TSF device) | 3.3 | 4282 | 25.8/14.7/5.9 | 24.7/7.7/1.7 | 14.4/8.4/3.3 | 480/57 | (0.138, 0.273) |

[a)]Voltage at 1 cd $m^{-2}$ (V); [b)]Maximum luminance (cd $m^{-2}$); Current efficiency (cd $A^{-1}$): maximum, values at 100 cd $m^{-2}$, 1000 cd $m^{-2}$; Power efficiency (lm $W^{-1}$): maximum, values at 100 cd $m^{-2}$, 1000 cd $m^{-2}$; External quantum efficiency (%): maximum, values at 100 cd $m^{-2}$, 1000 cd $m^{-2}$; [c)]The peak of the EL spectrum; Full width at half maximum of EL spectrum; [d)]Commission Internationale de l'Eclairage coordinates.

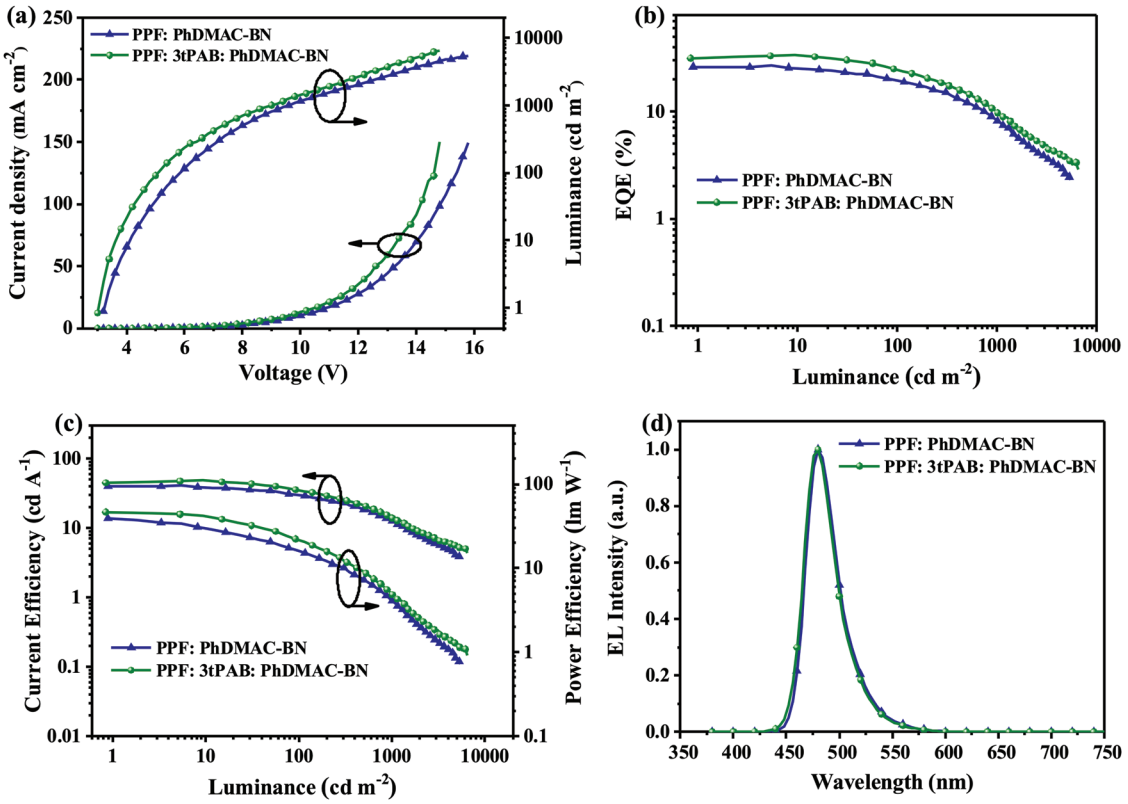


**Figure 5.** EL characteristics of the PhDMAC-BN with 5 wt.% doping concentration: a) Current density-voltage-brightness (*J–V–B*) characteristics. b) EQE-brightness curves. c) current efficiency-brightness-power efficiency curves. d) normalized EL spectra at 6 V.

PhDAMC-BN and PL spectra of 3tPAB demonstrated the possibility of FET (Figure S12a, Supporting Information). Subsequently, MR-TADF-sensitized MR-TADF devices were fabricated using the above device structure. As shown in Figure 5, at optimal doping concentration, the device efficiency exhibited significant improvement with the help of sensitizer 3tPAB. The $CE_{max}$, $PE_{max}$, and $EQE_{max}$ were improved from 41.5 cd $A^{-1}$, 39.2 lm $W^{-1}$, 27.2% to 48.1 cd $A^{-1}$, 46.6 lm $W^{-1}$, 33.9%. The external quantum efficiency roll-off of MR-TADF device with and without sensitizer was 71.4% and 69.9% at 1000 cd $m^{-2}$, respectively. Compared with the devices without sensitizer, the TST device exhibited similar efficiency roll-off. This can be attributed to the low $k_{RISC}$ rate constant ($2.39 \times 10^4$ $s^{-1}$) of the sensitizer. The $k_{RISC}$ value was in the same order of magnitude as MR-TADF emitter PhDMAC-BN ($5.04 \times 10^4$ $s^{-1}$). Therefore, the main effect of sensitizers was improving exciton utilization and enhancing the device efficiency. Similar results were also found in traditional fluorescence devices. It can be predicted that further increasing the $k_{RISC}$ of MR type TADF sensitizer by advanced molecular design can effectively reduce the efficiency roll-off. In addition, the emission wavelength and FWHM of the device were almost unchanged after the addition of 3tPAB, indicating the emission originated from PhDAMC-BN. It should be noted that our work was still at the advanced level in TADF-sensitized blue OLEDs in terms of device efficiency and color purity (Table S8, Supporting Information), although part of boron-based TADF material have been used as sensitizer for blue MR-TADF OLED and achieved excellent device efficiency and narrow FWHM.[18] To clarify the underlying causes of the boosted EL performance of the TST device, the transient PL spectra of PPF: 20 wt.% 3tPAB and PPF: 20 wt.% 3tPAB: 5 wt.% PhDAMC-BN films were measured (Figure S12b, Supporting Information). The reduced lifetime indicated the presence of FET between 3tPAB and PhDAMC-BN. Moreover, the similar PL spectrum or EL spectrum for PPF: 5 wt.% PhDAMC-BN and PPF: 20 wt.% 3tPAB: 5 wt.%

**Table 3.** The EL performances of PhDMAC-BN with 5 wt.% doping concentration.

| Compound | $V_{on}$[a)] ]V] | $L_{max}$[b)] ]cd $m^{-2}$] | $CE_{max}$[b)] ]cd $A^{-1}$] | $PE_{max}$[b)]lm $W^{-1}$] | $EQE_{max}$[b)] ]%] | $\lambda_{EL}$[c)] /FWHM[c)] ]nm] | CIE[d)] ]x, y] |
|---|---|---|---|---|---|---|---|
| PhDMAC-BN | 3.2 | 5398 | 41.5/29.9/12.5 | 39.2/16.2/4.1 | 27.2/19.7/8.2 | 480/34 | (0.105, 0.264) |
| PhDMAC-BN (TST device) | 3.1 | 6491 | 48.1/35.5/13.9 | 46.6/22.3/4.8 | 33.925.1/9.7 | 480/35 | (0.108, 0.223) |

[a)]Voltage at 1 cd $m^{-2}$ (V); [b)]Maximum luminance (cd $m^{-2}$); Current efficiency (cd $A^{-1}$): maximum, values at 100 cd $m^{-2}$, 1000 cd $m^{-2}$; Power efficiency (lm $W^{-1}$): maximum, values at 100 cd $m^{-2}$, 1000 cd $m^{-2}$; External quantum efficiency (%): maximum, values at 100 cd $m^{-2}$, 1000 cd $m^{-2}$; [c)]The peak of the EL spectrum; Full width at half maximum of EL spectrum; [d)]Commission Internationale de l'Eclairage coordinates.

PhDAMC-BN films demonstrated energy transfer was valid and complete. The corresponding $k_{FET}$ was calculated to be $8.21 \times 10^7$ $s^{-1}$ according to the reported method,[19] which was higher than above $7.23 \times 10^7$ $s^{-1}$ of the above TSF device (Table S7, Supporting Information). The higher $k_{FET}$ of the TST device was due to a slight red-shift absorption of PhDAMC-BN accounting for a larger spectral overlap between the emission of sensitizer and the absorption of the emitter. This also indicated that MR-TADF emitter with small Stokes shift can match MR-TADF sensitizer well compared with a traditional fluorescence emitter under the similar luminescence wavelength of the guest. Subsequently, the PLQY and Θ// of PPF: 20 wt.% 3tPAB: 5 wt.% PhDAMC-BN film were measured, exhibiting 97.0% and 98% (Figure S13, Supporting Information), respectively. These values were higher than that of PPF: 5 wt.% PhDAMC-BN film. Therefore, compared to the non-sensitized device, the enhanced performance of TST device can be attributed to efficient FET, improved PLQY, and higher Θ//.

In such TADF-sensitized device, the characteristics of the device also depended on the characteristics of the trap. Hole-only and electron-only devices were further prepared to determine the characteristics of charge trapping (Figure S14, Supporting Information). Because of the shallower LUMO energy levels of sensitizer (3tPAB) and emitters (PhDMAC-BN and DtPAPy) relative to the host (Figure S9, Supporting Information), electrons were transported through the host PPF in TSF and TST devices (Figure S14a, Supporting Information). In addition, comparable and shallow HOMO energy levels of sensitizer 3tPAB and emitter PhDMAC-BN were found. The deep hole traps and high doping concentrations of sensitizer made the injected holes primarily captured by the sensitizer in the TST device (Figure S14b, Supporting Information). However, in the TSF device, due to the higher doping concentration of the sensitizer and the shallower HOMO level of emitter DtPAPy relative to the sensitizer, the injected holes were captured by both the sensitizer and the emitter. This was why the current density of the hole-only device for the TSF device was almost coincided with the device with sensitizer only at low voltage and slightly increased at high voltage. Such charge trapping features can also be verified by the characteristics of the current density-voltage (*J*–*V*) curve of MR-TADF sensitized and non-sensitized devices (Figures S7a, S8a, S10a, and Figure S11a, Supporting Information). After the MR-TADF sensitizer was added, the *J*–*V* curves of the TST device showed almost unchanged as the concentration of the guest increased, while the *J*–*V* curves variation of the TSF device were suppressed in total but slightly changed. In short, from the results of TSF and TST devices, it can be seen that the new sensitizer 3tPAB played an important role in improving device performance. Nevertheless, the fast reverse intersystem crossing rate and aligned molecular orbital levels with the emitter were still required for the ideal MR-TADF sensitizer, which can suppress the triplet-related quenching process and minimize carrier trapping by the fluorescent emitter. To our knowledge, this is the first report using MR-TADF emitter as sensitizer, which will broaden the application range of MR-TADF materials.

## 3. Conclusion

In summary, a deep-blue MR-TADF emitter 3tPAB with weak concentration dependence was used as sensitizer for the improvement of blue OLED. The traditional blue fluorescence device using 3tPAB as sensitizer achieved $EQE_{max}$ of 14.4%. The quantum efficiency was enhanced by ≈2.4 times compared to the non-sensitized reference device. In addition, given the excellent TADF properties, narrow emission, and high PLQY of the new synthesized MR-TADF compound, the device based on PhDMAC-BN as emitter achieved $EQE_{max}$ of 27.2%, FWHM of 34 nm, and CIE coordinates of (0.105, 0.264), respectively. More importantly, the $EQE_{max}$ was further improved to 33.9% when 3tPAB was employed as sensitizer for PhDMAC-BN. Because of efficient and complete Förster energy transfer, the high color purity of the device was maintained. Therefore, the work first demonstrated the feasibility of MR-TADF as sensitizer and provided a new strategy to improve the performance of blue OLED. We believe this strategy will bring a useful reference to improve the performance of other color devices.

## Supporting Information

Supporting Information is available from the Wiley Online Library or from the author.

## Acknowledgements

This work was supported by the National Natural Science Foundation of China (62004074, 51727809), and the Science and Technology Department of Hubei Province (2021AAA008, 2020BAA016, 2019AAA063). Wuhan Science and Technology Bureau (2019010701011406). Thanks to SCTS/CGCL HPCC of HUST for providing computing resources and technical support. The Analytical and Testing Center at Huazhong University of Science and Technology is acknowledged for the characterization of new compounds.

## Conflict of Interest

The authors declare no conflict of interest.

## Data Availability Statement

The data that support the findings of this study are available from the corresponding author upon reasonable request.

## Keywords

boron derivatives, multiple resonance effects, organic light-emitting diodes, sensitizer, thermally activated delayed fluorescence

Received: September 13, 2022
Published online: October 31, 2022

[1] a) D. Zhang, T. Huang, L. Duan, *Adv. Mater.* **2020**, *32*, 1902391; b) Z. Xu, B. Z. Tang, Y. Wang, D. Ma, *J. Mater. Chem. C* **2020**,

 

*8*, 2614; c) W. Song, I. Lee, J. Y. Lee, *Adv. Mater.* **2015**, *27*, 4358; d) H. Lim, H. J. Cheon, S.-J. Woo, S.-K. Kwon, Y.-H. Kim, J.-J. Kim, *Adv. Mater.* **2020**, *32*, 2004083; e) T.-L. Wu, M.-J. Huang, C.-C. Lin, P.-Y. Huang, T.-Y. Chou, R.-W. Chen-Cheng, H.-W. Lin, R.-S. Liu, C.-H. Cheng, *Nat. Photonics* **2018**, *12*, 235; f) Z. Xu, J. Gu, X. Qiao, A. Qin, B. Z. Tang, D. Ma, *ACS Photonics* **2019**, *6*, 767; g) P. Han, C. Lin, D. Ma, A. Qin, B. Z. Tang, *ACS Appl. Mater. Interfaces* **2020**, *12*, 46366; h) Y.-L. Zhang, Q. Ran, Q. Wang, Y. Liu, C. Hänisch, S. Reineke, J. Fan, L.-S. Liao, *Adv. Mater.* **2019**, *31*, 1902368.

[2] a) K. Stavrou, S. Madayanad Suresh, D. Hall, A. Danos, N. A. Kukhta, A. M. Z. Slawin, S. Warriner, D. Beljonne, Y. Olivier, A. Monkman, E. Zysman-Colman, *Adv. Opt. Mater.* **2022**, *10*, 2200688; b) J.-M. Teng, Y.-F. Wang, C.-F. Chen, *J. Mater. Chem. C* **2020**, *8*, 11340; c) S. Madayanad Suresh, D. Hall, D. Beljonne, Y. Olivier, E. Zysman-Colman, *Adv. Funct. Mater.* **2020**, *30*, 1908677; d) T. Fan, Y. Zhang, D. Zhang, L. Duan, *Chem. - Eur. J.* **2022**, *28*, e2021046; e) A. Khan, X. Tang, C. Zhong, Q. Wang, S.-Y. Yang, F.-C. Kong, S. Yuan, A. S. D. Sandanayaka, C. Adachi, Z.-Q. Jiang, L.-S. Liao, *Adv. Funct. Mater.* **2021**, *31*, 2009488; f) J.-J. Hu, X.-F. Luo, Y.-P. Zhang, M.-X. Mao, H.-X. Ni, X. Liang, Y.-X. Zheng, *J. Mater. Chem. C* **2022**, *10*, 768; g) X. F. Luo, H. X. Ni, H. L. Ma, Z. Z. Qu, J. Wang, Y. X. Zheng, J. L. Zuo, *Adv. Opt. Mater.* **2022**, *10*, 2102513.

[3] X. F. Luo, F. L. Li, J. W. Zou, Q. Zou, J. Su, M. X. Mao, Y. X. Zheng, *Adv. Opt. Mater.* **2021**, *9*, 2100784.

[4] Y. Kondo, K. Yoshiura, S. Kitera, H. Nishi, S. Oda, H. Gotoh, Y. Sasada, M. Yanai, T. Hatakeyama, *Nat. Photonics* **2019**, *13*, 678.

[5] a) X. Yang, X. Xu, G. Zhou, *J. Mater. Chem. C* **2015**, *3*, 913; b) X. Cai, S.-J. Su, *Adv. Funct. Mater.* **2018**, *28*, 1802558; c) W. J. Chung, K. H. Lee, M. Jung, K. M. Lee, H. C. Park, M. S. Eum, J. Y. Lee, *Adv. Opt. Mater.* **2021**, *9*, 2100203; d) H.-J. Tan, G.-X. Yang, Y.-L. Deng, C. Cao, J.-H. Tan, Z.-L. Zhu, W.-C. Chen, Y. Xiong, J.-X. Jian, C.-S. Lee, Q.-X. Tong, *Adv. Mater.* **2022**, *34*, 2200537; e) Y. Wang, J. H. Yun, L. Wang, J. Y. Lee, *Adv. Funct. Mater.* **2021**, *31*, 2008332; f) S. K. Jeon, H. L. Lee, K. S. Yook, J. Y. Lee, *Adv. Mater.* **2019**, *31*, 1803524.

[6] a) J. Wei, C. Zhang, D. Zhang, Y. Zhang, Z. Liu, Z. Li, G. Yu, L. Duan, *Angew. Chem., Int. Ed.* **2021**, *60*, 12269; b) H. L. Lee, W. J. Chung, J. Y. Lee, *Small* **2020**, *16*, 1907569; c) V. V. Patil, K. H. Lee, J. Y. Lee, *J. Mater. Chem. C* **2020**, *8*, 3051; d) G. Meng, D. Zhang, J. Wei, Y. Zhang, T. Huang, Z. Liu, C. Yin, X. Hong, X. Wang, X. Zeng, D. Yang, D. Ma, G. Li, L. Duan, *Chem. Sci.* **2022**, *13*, 5622; e) Y. Wang, K. Di, Y. Duan, R. Guo, L. Lian, W. Zhang, L. Wang, *Chem. Eng. J.* **2022**, *431*, 133221.

[7] a) Y. Wada, H. Nakagawa, S. Matsumoto, Y. Wakisaka, H. Kaji, *Nat. Photonics* **2020**, *14*, 643; b) L.-S. Cui, A. J. Gillett, S.-F. Zhang, H. Ye, Y. Liu, X.-K. Chen, Z.-S. Lin, E. W. Evans, W. K. Myers, T. K. Ronson, H. Nakanotani, S. Reineke, J.-L. Bredas, C. Adachi, R. H. Friend, *Nat. Photonics* **2020**, *14*, 636; c) S. O. Jeon, K. H. Lee, J. S. Kim, S.-G. Ihn, J. W. Kim, H. Lee, S. Kim, H. Choi, J. Y. Lee, Y. S. Chung, *Nat. Photonics* **2021**, *15*, 208; d) D. Zhang, X. Song, A. J. Gillett, B. H. Drummond, S. T. E. Jones, G. Li, H. He, M. Cai, D. Credgington, L. Duan, *Adv. Mater.* **2020**, *32*, 1908355; e) D. H. Ahn, J. H. Jeong, J. Song, J. Y. Lee, J. H. Kwon, *ACS Appl. Mater. Interfaces* **2018**, *10*, 10246.

[8] H. Nakanotani, T. Higuchi, T. Furukawa, K. Masui, K. Morimoto, M. Numata, H. Tanaka, Y. Sagara, T. Yasuda, C. Adachi, *Nat. Commun.* **2014**, *5*, 4016.

[9] I. H. Lee, W. Song, J. Y. Lee, S.-H. Hwang, *J. Mater. Chem. C* **2015**, *3*, 8834.

[10] S. H. Han, J. H. Jeong, J. W. Yoo, J. Y. Lee, *J. Mater. Chem. C* **2019**, *7*, 3082.

[11] a) C.-Y. Chan, M. Tanaka, Y.-T. Lee, Y.-W. Wong, H. Nakanotani, T. Hatakeyama, C. Adachi, *Nat. Photonics* **2021**, *15*, 203; b) R. K. Konidena, J. Lim, J. Y. Lee, *Chem. Eng. J.* **2021**, *416*, 129097; c) X. Lv, J. Miao, M. Liu, Q. Peng, C. Zhong, Y. Hu, X. Cao, H. Wu, Y. Yang, C. Zhou, J. Ma, Y. Zou, C. Yang, *Angew. Chem., Int. Ed.* **2022**, *61*, e202201588; d) X. Wang, Y. Zhang, H. Dai, G. Li, M. Liu, G. Meng, X. Zeng, T. Huang, L. Wang, Q. Peng, D. Yang, D. Ma, D. Zhang, L. Duan, *Angew. Chem., Int. Ed.* **2022**, *61*, e202206916.

[12] T. Hatakeyama, K. Shiren, K. Nakajima, S. Nomura, S. Nakatsuka, K. Kinoshita, J. Ni, Y. Ono, T. Ikuta, *Adv. Mater.* **2016**, *28*, 2777.

[13] a) M. Yang, I. S. Park, T. Yasuda, *J. Am. Chem. Soc.* **2020**, *142*, 19468; b) X. Liang, Z.-P. Yan, H.-B. Han, Z.-G. Wu, Y.-X. Zheng, H. Meng, J.-L. Zuo, W. Huang, *Angew. Chem., Int. Ed.* **2018**, *57*, 11316.

[14] I. S. Park, H. Min, T. Yasuda, *Angew. Chem., Int. Ed.* **2022**, *61*, e202205684.

[15] a) Y. Wang, Y. Duan, R. Guo, S. Ye, K. Di, W. Zhang, S. Zhuang, L. Wang, *Org. Electron.* **2021**, *97*, 106275; b) P. Heimel, A. Mondal, F. May, W. Kowalsky, C. Lennartz, D. Andrienko, R. Lovrincic, *Nat. Commun.* **2018**, *9*, 4990.

[16] a) T. Förster, *Discuss. Faraday Soc.* **1959**, *27*, 7; b) A. R. Clapp, I. L. Medintz, H. Mattoussi, *ChemPhysChem* **2006**, *7*, 47.

[17] a) Q. Zhang, H. Kuwabara, J. William, J. Potscavage, S. Huang, Y. Hatae, T. Shibata, C. Adachi, *J. Am. Chem. Soc.* **2014**, *136*, 18070; b) Q. Zhang, B. Li, S. Huang, H. Nomura, H. Tanaka, C. dachi, *Nat. Photonics* **2014**, *8*, 326; c) H. Kaji, H. Suzuki, T. Fukushima, K. Shizu, K. Suzuki, S. Kubo, T. Komino, H. Oiwa, F. Suzuki, A. Wakamiya, Y. Murata, C. Adachi, *Nat. Commun.* **2015**, *6*, 8476.

[18] a) K. R. Naveen, H. Lee, R. Braveenth, D. Karthik, K. J. Yang, S. J. Hwang, J. H. Kwon, *Adv. Funct. Mater.* **2022**, *32*, 2110356; b) R. Braveenth, H. Lee, J. D. Park, K. J. Yang, S. J. Hwang, K. R. Naveen, R. Lampande, J. H. Kwon, *Adv. Funct. Mater.* **2021**, *31*, 2105805.

[19] X. Song, D. Zhang, Y. Zhang, Y. Lu, L. Duan, *Adv. Opt. Mater.* **2020**, *8*, 2000483.

ADVANCED OPTICAL MATERIALS

# Supporting Information

for *Adv. Optical Mater.,* DOI: 10.1002/adom.202202034

## Multiple-Resonance-Type TADF Emitter as Sensitizer Improving the Performance of Blue Fluorescent Organic Light-Emitting Diodes

*Yaxiong Wang, Runda Guo,* Ao Ying, Kaiyuan Di, Linya Chen, Honggang Gu, Shiyuan Liu, Yalei Duan, Hanrui Su, Shaolong Gong, and Lei Wang**

Supporting Information

# MR-TADF Emitter as Sensitizer Improving the Performance of Blue Fluorescent Organic Light-Emitting Diodes

Yaxiong Wang [a], Runda Guo*[a], Ao Ying [b], Kaiyuan Di [a], Linya Chen [c], Honggang Gu [d], Shiyuan Liu [d], Yalei Duan [a], Hanrui Su [a], Shaolong Gong [b], Lei Wang*[a]

[a] *Wuhan National Laboratory for Optoelectronics, Huazhong University of Science and Technology, Wuhan, 430074, People's Republic of China.*

[b] *Hubei Key Lab on Organic and Polymeric Optoelectronic Materials Department of Chemistry, Wuhan University, Wuhan 430072, People's Republic of China.*

[c] *School of Optical and Electronic Information, Huazhong University of Science and Technology, Wuhan, 430074, People's Republic of China.*

[d] *State Key Laboratory of Digital Manufacturing Equipment and Technology, Huazhong University of Science and Technology, Wuhan, 430074, People's Republic of China.*

**Corresponding Author**

[*]*Email: wanglei@mail.hust.edu.cn*

[*]*Email: runda_guo@hust.edu.cn.*

**Characterization.**

The intermediates and final compounds were confirmed by $^{1}H$ NMR or $^{13}C$ NMR spectra on a Bruker-AF301 AT 400 or 600 MHz spectrometer. Mass spectra were recorded on high resolution Fourier-transform mass spectrometer. Differential scanning calorimetry (DSC) was measured under nitrogen on a PE Instruments DSC 2920 unit at a heating rate of 10 °C $min^{-1}$ from 30 to 400 °C. The glass transition temperature ($T_g$) was determined from the second heating scan. Thermogravimetric analysis (TGA) was undertaken using a PerkinElmer Instruments Pyris1 TGA at a heating rate of 10 °C $min^{-1}$ from 30 to 600 °C under a nitrogen atmosphere. The thermal decomposition temperatures ($T_d$) were corresponded to 5% weight loss temperatures. The UV-vis absorption spectra were measured on a Shimadzu UV-VIS-NIR Spectrophotometer (UV-3600) in the wavelength range of 190-1100 nm. The PL spectra and the transient photoluminescence spectra were recorded on an Edinburgh Instruments (FLS 920 spectrometer). The absolute PLQY tests were carried out using a Zolix OmniFluo spectrofluorometer equipped with a calibrated integrating sphere. Cyclic voltammetry was recorded on a computer-controlled EG&G Potentiostat/Galvanostat model 283 at room temperature with a conventional three-electrode system, which consisted of a platinum wire counter electrode, $Ag/AgNO_3$ (0.1 M) reference electrode, and a glassy carbon working electrode of 2 mm diameter. A 0.10 M tetrabutylammonium hexafluorophosphate (*n*-$Bu_4NPF_6$) solutions in dry dichloromethane was employed as the supporting electrolyte, and ferrocene was added as a calibrant in the whole measurement.

**Device fabrication and measurements.**

The used ITO glass substrates, $MoO_3$, LiF, TAPC, *m*CP, PPF, and TmPyPB were commercially available. The devices were fabricated by evaporating organic layers on ITO (20 Ω $square^{-1}$), which were precleaned carefully and treated with oxygen plasma for 5 min. The devices were deposited in the vacuum of $2 \times 10^{-6}$ Torr. For all of the OLEDs, the emitting areas were determined by the overlap of two electrodes as 0.09 $cm^2$. The *J-V-L* of the devices was measured using a Keithley 2400 source meter

equipped with a calibrated silicon photodiode. The EL spectra were measured using a PR655 spectrometer. All measurements were carried out at room temperature under ambient conditions.

**Calculation details.**

The density functional theory (DFT) and timed dependent DFT (TD-DFT) calculations were employed to optimize the ground state and excited state geometries and electronic properties, which were carried out with the B3LYP hybrid functional at the basis set level of 6-31G(d).

**Calculation Formulas for the Photophysical Parameters**

The evaluations of exciton dynamic rate constants were calculated by equation S1-S6 [1]:

$k_p = 1/\tau_{PF}$ Equation S1

$k_d = 1/\tau_{DF}$ Equation S2

$k_F = \Phi_{PF}/\tau_{PF}$ Equation S3

$\Phi = k_F/(k_F + k_{IC})$ Equation S4

$\Phi_{PF} = k_F/(k_F + k_{IC} + k_{ISC})$ Equation S5

The total PLQY of the emitter-doped PPF films is high enough. And phosphorescence was not observed at room temperature. Therefore, it is reasonably assumed that 1) $k_r^S \gg k_{nr}^S, k_r^T, k_{nr}^T$ and 2) $k_{RISC} \gg k_r^T, k_{nr}^T$. Where $k_r^S$ and $k_{nr}^S$ are the rate constants for radiative and non-radiative decay from $S_1$, $k_r^T$ and $k_{nr}^T$ are the rate constants of radiative and non-radiative decay from $T_1$, respectively. It is experimentally observed that $k_p \gg k_d$(Table.S3), then $k_p \approx k_r + k_{ISC} + k_{RISC}$ and $k_p k_d \approx k_r k_{RISC}$. When $k_{ISC} \gg k_{RISC}$, $k_p$ can be expressed as $k_p \approx k_r + k_{ISC}$, and $k_{RISC}$ is obtained as:

$k_{RISC} = k_p k_d/(k_p - k_{ISC})$ Equation S6

**Molecular synthesis**

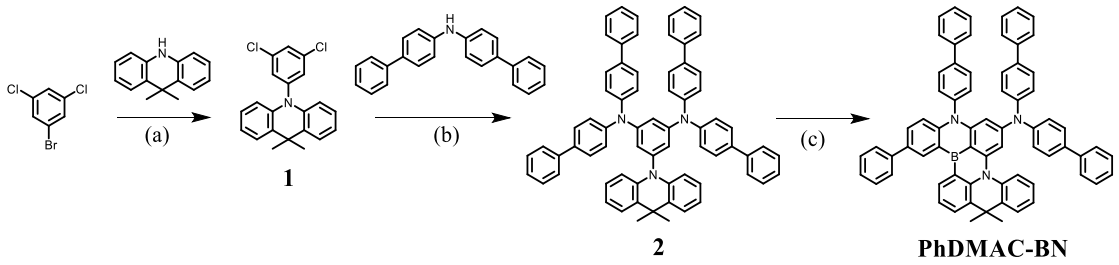


**Scheme S1.** Synthetic Routes: (a) $Pd(OAc)_2$, $P(tBu)_3{\cdot}HBF_4$, NaOt-Bu, Toluene, 120 ℃, 24 h, $N_2$; (b) $Pd_2(dba)_3$, Sphos, NaOt-Bu, Toluene, 110 ℃,18 h, $N_2$; (c) $BBr_3$, DIPEA, 180 ℃, 20h, $N_2$.

10-(3,5-dichlorophenyl)-9,9-dimethyl-9,10-dihydroacridine (1): The mixture of 1-bromo-3,5-dichlorobenzene (3.56 g, 15.80 mmol), 9,9-dimethyl-9,10-dihydroacridine (3.00g, 14.30 mmol), $Pd(OAc)_2$ (0.16 g, 0.72 mmol), $P(t\text{-}Bu)_3{\cdot}HBF_4$ (0.25 g, 0.86 mmol) and *t*-BuONa (4.10 g, 42.90 mmol) was added to the toluene (60 mL). The mixture was stirred at 120 °C for 24 h under $N_2$ atmosphere. After the reaction mixture was cooled to room temperature, toluene was removed in vacuo. Then the resulting mixture was extracted by water and dichloromethane for three times. The organic layer was dried by $MgSO_4$, then filtered and concentrated under reduced pressure. Finally, the crude product was purified by column chromatography (elution solvent: petroleum ether) to afford a white solid (2.8 g). Yield, 55%. $^1$H NMR (400 MHz, $CDCl_3$) $\delta$ [ppm]: $\delta$ 7.56 – 7.51 (m, 1H), 7.50 – 7.44 (m, 2H), 7.30 (d, $J$ = 1.7 Hz, 2H), 7.07 – 6.93 (m, 4H), 6.29 (d, $J$ = 8.0 Hz, 2H), 1.68 (s, 6H).

*N*1,*N*1,*N*3,*N*3-tetra([1,1'-biphenyl]-4-yl)-5-(9,9-dimethylacridin-10(9*H*)-yl)benzene-1,3-diamine (2): The mixture of intermediate product 1 (2.60 g, 7.30 mmol), di([1,1'-biphenyl]-4-yl)amine (5.19 g, 16.10 mmol), $Pd_2(dba)_3$ (0.067 g, 0.073 mmol), SPhos (0.06 g, 0.146 mmol) and *t*-BuONa (2.10 g, 21.90 mmol) was dissolved in toluene (70 mL). And the mixture refluxed at 110 °C for 18 h under $N_2$ atmosphere. After reaction finished, toluene was removed by vacuum distillation. Then the crude product was extracted by water and dichloromethane for three times. The organic layer was dried by $MgSO_4$, then filtered and concentrated in vacuo. Finally, the crude

product was purified by column chromatography (elution solvent: petroleum ether/ dichloromethane = 20/1) and further recrystallized by dichloromethane and methanol to afford a white solid (5.8g). Yield, 86%. $^{1}$H NMR (400 MHz, DMSO) $\delta$ [ppm]: $\delta$ 7.65 (d, $J$ = 8.6 Hz, 8H), 7.58 (d, $J$ = 7.2 Hz, 8H), 7.40 (dd, $J$ = 16.1, 9.0 Hz, 10H), 7.31 (dd, $J$ = 17.1, 7.9 Hz, 12H), 7.14 (dd, $J$ = 11.4, 4.2 Hz, 2H), 6.94 – 6.83 (m, 3H), 6.58 (d, $J$ = 8.2 Hz, 2H), 6.49 (d, $J$ = 2.0 Hz, 2H), 1.50 (s, 6H).

*N*,*N*,8-tri([1,1'-biphenyl]-4-yl)-16,16-dimethyl-11-phenyl-8*H*,16*H*-4b,8-diaza-12 b-boradibenzo[a,j]perylen-6-amine (PhDMAC-BN): Boron tribromide (0.83 mL, 8.66 mmol) was added to a solution of 2 (2.5 g, 2.71 mmol) in *o*-dichlorobenzene (0 mL) at room temperature under a nitrogen atmosphere. After stirring at 180 ºC for 20 h, the reaction mixture was allowed to cool to 0 ℃. After addition of *N*, *N*-diisopropylethylamine (5.37 mL, 32.52 mmol), the reaction mixture was stirred at 0 ℃ for 0.5 h. Then, an aqueous solution of sodium acetate (0.1 g/mL) was added. The PH of reaction mixture was regulated to neutral value. The aqueous layer was separated and extracted with dichloromethane. The combined organic layers were dried with $MgSO_4$, filtered, and evaporated under reduced pressure. Then, *o*-dichlorobenzene was further removed by reduced pressure distillation at 70 ºC. The crude product was further purified by column chromatography (elution solvent: petroleum ether/ dichloromethane = 9/1) and subsequently recrystallized by toluene and methanol to afford a yellow solid (1.1 g). Yield, 44%. $^{1}$H NMR (600 MHz, $CD_2Cl_2$) $\delta$ [ppm]: $\delta$ 9.05 (s, 1H), 8.66 (d, $J$ = 7.4 Hz, 1H), 7.83 – 7.72 (m, 6H), 7.68 (d, $J$ = 7.9 Hz, 1H), 7.61 – 7.29 (m, 26H), 7.24 (d, $J$ = 8.3 Hz, 4H), 7.21 – 7.13 (m, 3H), 7.09 (d, $J$ = 8.9 Hz, 1H), 5.98 (s, 1H), 2.03 (s, 3H), 1.37 (s, 3H). $^{13}$C NMR (151 MHz, $CD_2Cl_2$) $\delta$ [ppm]: $\delta$ 150.56, 147.53, 147.06, 146.06, 145.01, 143.64, 141.60, 141.14, 140.77, 140.63, 140.32, 140.01, 138.24, 136.34, 135.52, 133.10, 132.62, 132.36, 129.91, 128.82, 128.78, 128.75, 127.61, 127.54, 127.10, 126.96, 126.87, 126.65, 126.60, 125.74, 125.43, 124.31, 123.79, 122.60, 119.75, 117.46, 103.81, 102.09, 37.04, 30.78, 22.79. FTMS (APCI, m/z): calculated for $C_{69}H_{50}BN_3$, 931.9900; found, 932.4179.

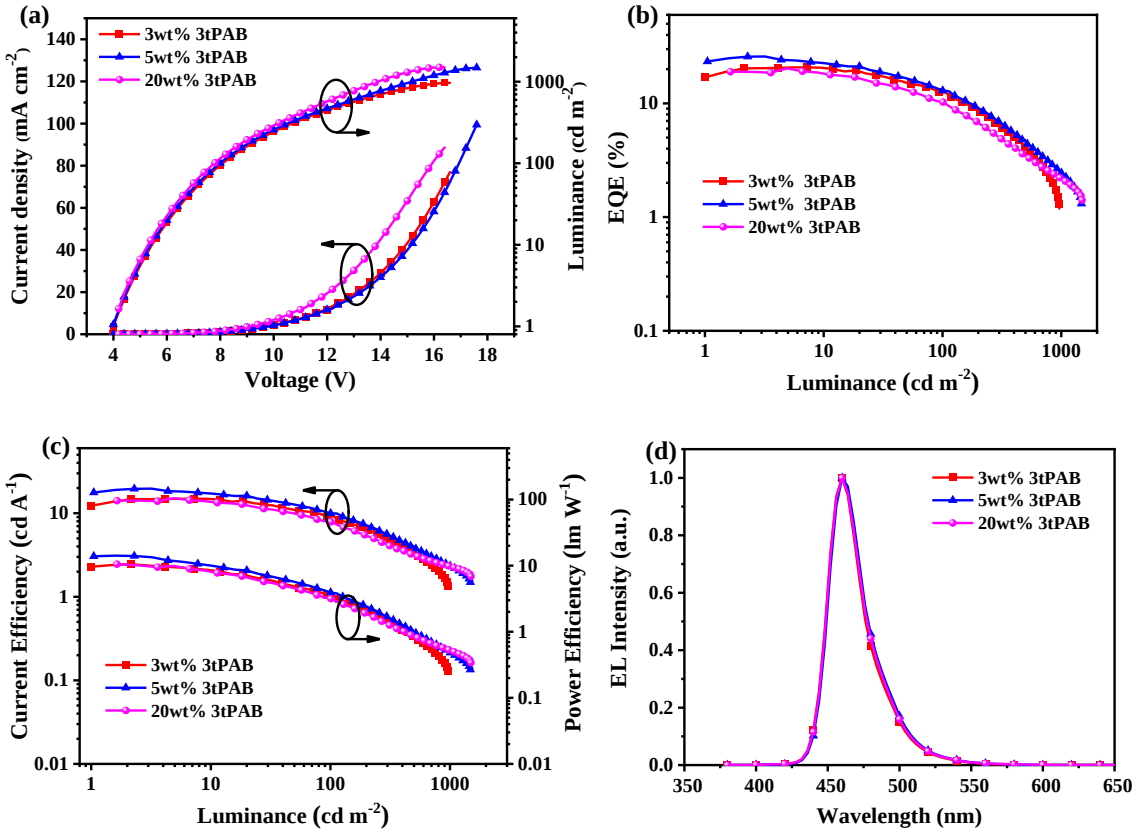


**Figure S1.** EL characteristics of 3tPAB-based device: (a) Current density-voltage-brightness (J-V-B) characteristics; (b) EQE-brightness curves; (c) current efficiency-brightness-power efficiency curves; (d) normalized EL spectra at 6 V. The device structures were ITO/$MoO_3$ (10 nm)/TAPC (60 nm)/mCP (10 nm)/PPF: xwt%3tPAB (20 nm, x=3, 5, 20)/PPF (10 nm)/TmPyPB (30 nm)/LiF (1 nm)/Al (100 nm).

**Table S1** The EL performances of 3tPAB.

| Compound | $V_{on}$[a] (V) | $L_{max}$[b] (cd $m^{-2}$) | $CE_{max}$[b] (cd $A^{-1}$) | $PE_{max}$[b](lm $W^{-1}$) | $EQE_{max}$[b] (%) | $\lambda_{EL}$[c] /FWHM[c] (nm) | CIE[d] (x, y) |
|---|---|---|---|---|---|---|---|
| 3tPAB(3wt%) | 4.0 | 965 | 14.9 | 10.5 | 20.7 | 460/28 | (0.134, 0.078) |
| 3tPAB(5wt%) | 4.0 | 1483 | 19.6 | 14.2 | 25.8 | 460/29 | (0.132, 0.085) |
| 3tPAB(20wt%) | 4.1 | 1500 | 14.1 | 10.6 | 20.3 | 460/29 | (0.134, 0.082) |

[a)] Voltage at 1 cd $m^{-2}$ (V); [b)] Maximum luminance (cd $m^{-2}$); Maximum current efficiency (cd $A^{-1}$); Maximum power efficiency (lm $W^{-1}$); Maximum external quantum efficiency (%); [c)] The peak of the EL spectrum; Full width at half maximum of EL spectrum; [d)] Commission Internationale de l'Eclairage coordinates.

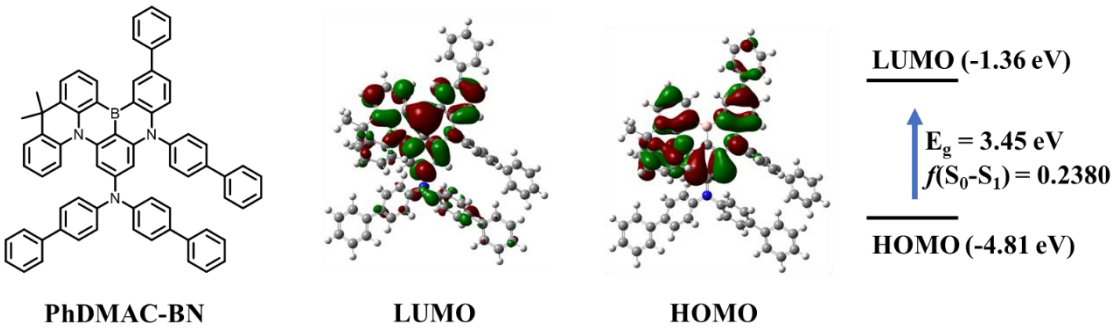


**Figure S2.** Distributions of frontier molecular orbitals of PhDMAC-BN.

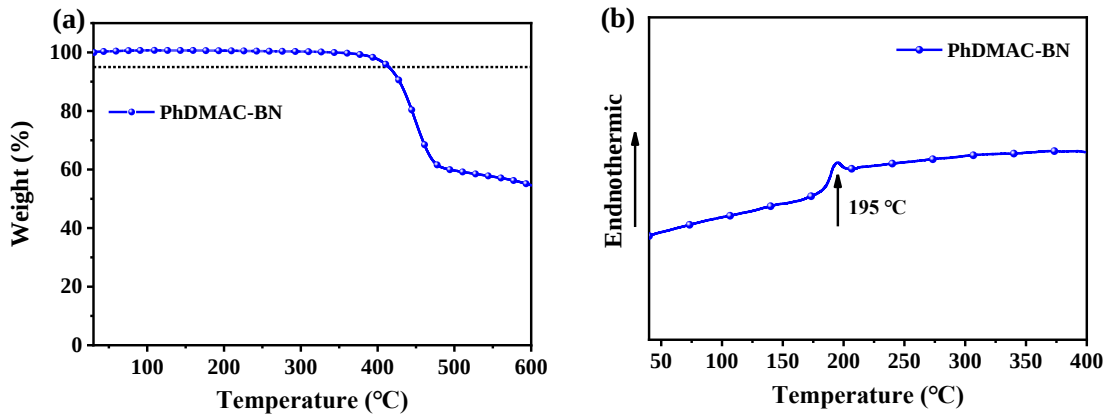


**Figure S3.** (a) TGA and (b) DSC curves of PhDMAC-BN.

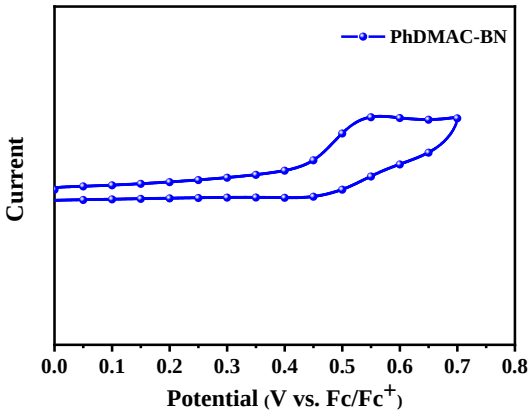


**Figure S4.** Cyclic voltammogram of PhDMAC-BN.

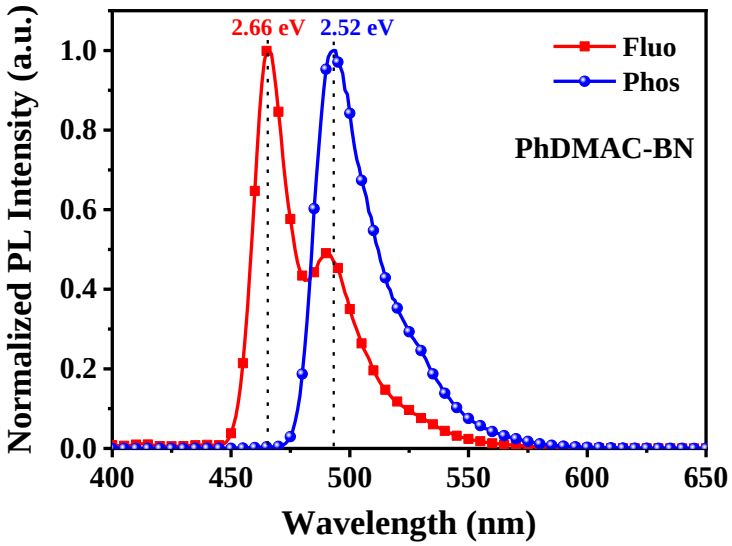


**Figure S5**. The low-temperature (77K) fluorescence and phosphorescence spectra of PhDMAC-BN in toluene.

**Table S2** The photophysical data of PhDMAC-BN in different solvents.

| Compound | Fluorescence | Cyclohexane | Toluene | Dichloromethane | *N*,*N*-dimethylformamide |
|---|---|---|---|---|---|
| PhDMAC-BN | $\lambda^{a}_{em}$ (nm) | 467 | 473 | 480 | 479 |
| | FWHM[b] (nm) | 24 | 27 | 33 | 33 |

[a)] the peak wavelength of the PL spectrum; [b)] Full width at half maximum.

**Table S3.** the photophysical parameter PhDMAC-BN (5wt% doped in PPF).

| compound | $\Phi/\Phi_{PF}/\Phi_{DF}$ | $\tau_{PF}$(ns)/$\tau_{DF}$(μs) | $k_p$ ($10^8$ $s^{-1}$) | $k_d$ ($10^4$ $s^{-1}$) | $k_F$ ($10^7$ $s^{-1}$) | $k_{IC}$ ($10^7$ $s^{-1}$) | $k_{ISC}$ ($10^7$ $s^{-1}$) | $k_{RISC}$ ($10^4$ $s^{-1}$) |
|---|---|---|---|---|---|---|---|---|
| PhDMAC-BN | 0.864/0.619/0.245 | 6.2/27.7 | 1.61 | 3.61 | 9.98 | 1.57 | 4.57 | 5.04 |

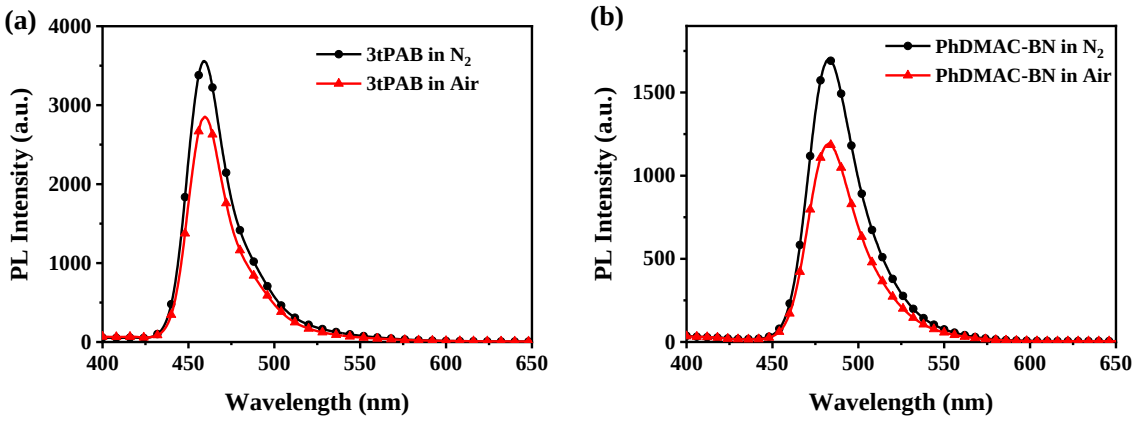


**Figure S6.** Degassed vs aerated fluorescence spectra of 3tPAB and PhDMAC-BN in PPF at room temperature.

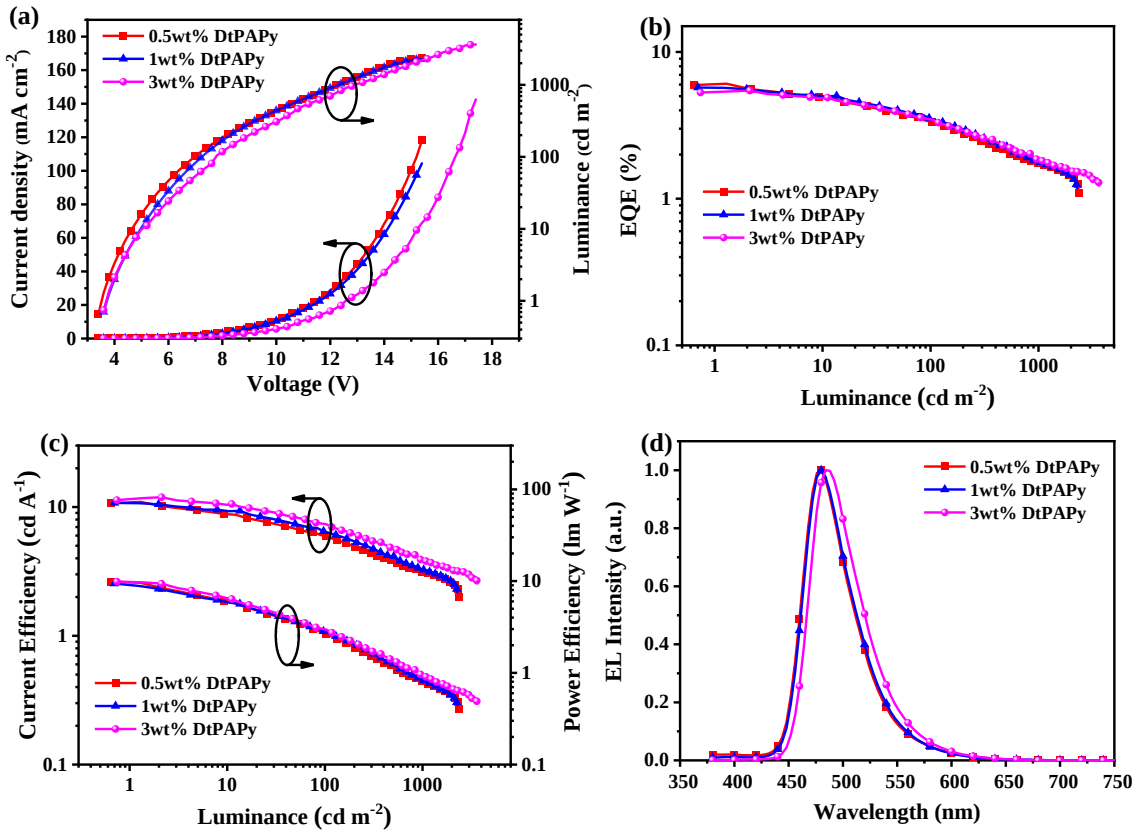


**Figure S7.** EL characteristics of the DtPAPy in non-sensitized OLED with structures of ITO/ $MoO_3$ (10 nm)/ TAPC (60 nm)/ mCP (10 nm)/ PPF: x wt% DtPAPy (20 nm, x=0.5, 1, 3)/ PPF (10 nm)/ TmPyPB (30 nm)/ LiF (1 nm)/ Al (100 nm). a) Current density–voltage-brightness (J-V-B) characteristics. b) EQE-brightness curves. c) current efficiency-brightness-power efficiency curves. d) normalized EL spectra at 6 V.

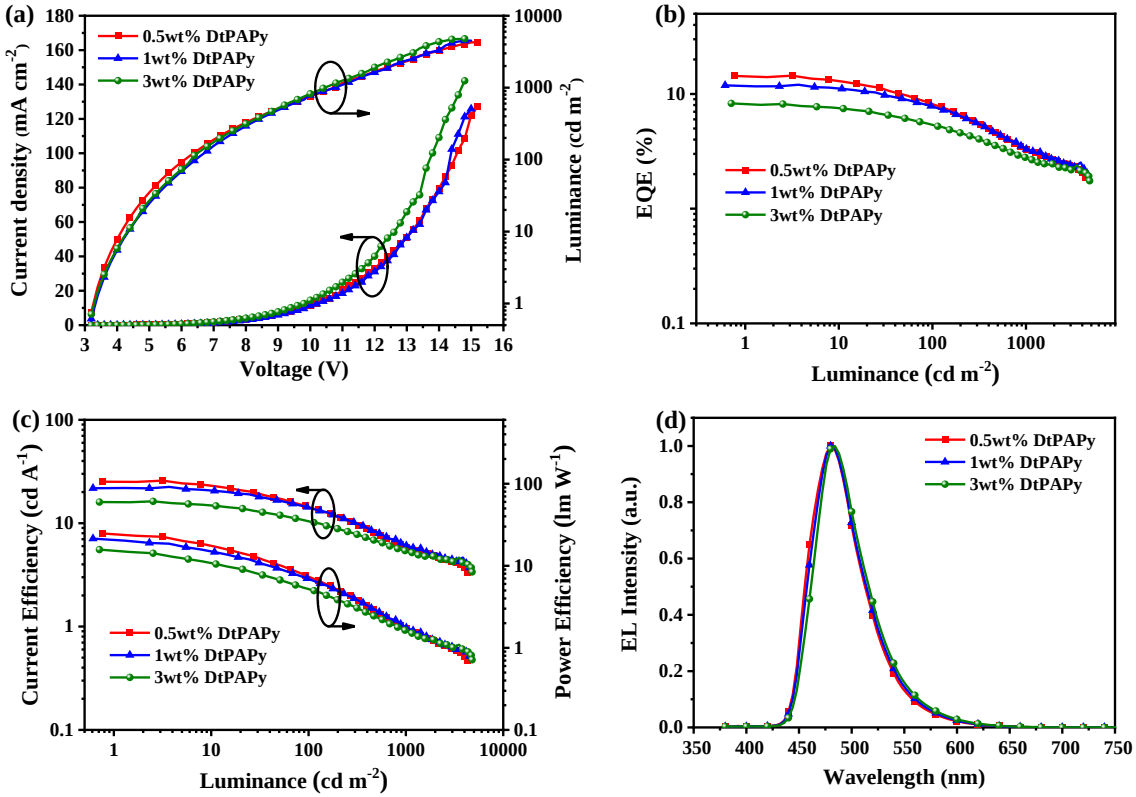


**Figure S8.** EL characteristics of the DtPAPy in TADF-sensitized OLED with structures of ITO/ $MoO_3$ (10 nm)/ TAPC (60 nm)/ mCP (10 nm)/ PPF: 20wt% 3tPAB: x wt% DtPAPy (20 nm, x=0.5, 1, 3)/ PPF (10 nm)/ TmPyPB (30 nm)/ LiF (1 nm)/ Al (100 nm). a) Current density-voltage-brightness (J-V-B) characteristics. b) EQE-brightness curves. c) current efficiency-brightness-power efficiency curves. d) normalized EL spectra at 6 V.

**Table S4** The EL performances of DtPAPy in non-sensitized OLED TADF-sensitized OLED.

| Compound | $V_{on}$ [a] (V) | $L_{max}$ [b] (cd $m^{-2}$) | $CE_{max}$ [b] (cd $A^{-1}$) | $PE_{max}$ [b](lm $W^{-1}$) | $EQE_{max}$ [b] (%) | $\lambda_{EL}$ [c] /FWHM[c] (nm) | CIE[d] (x, y) |
|---|---|---|---|---|---|---|---|
| DtPAPy (0.5wt%) | 3.5 | 2348 | 11.0/5.9/3.2 | 9.9/2.6/0.8 | 6.1/3.3/1.7 | 480/51 | (0.139, 0.289) |
| DtPAPy (1wt%) | 3.7 | 2277 | 10.7/6.5/3.3 | 9.4/2.8/0.8 | 5.7/3.5/1.8 | 480/52 | (0.138, 0.304) |
| DtPAPy (3wt%) | 3.7 | 3063 | 11.9/7.3/3.9 | 9.9/2.9/0.9 | 5.5/3.5/1.9 | 484/54 | (0.145, 0.384) |
| DtPAPy (0.5wt%) TSF-Device | 3.3 | 4282 | 25.8/14.7/5.9 | 24.7/7.7/1.7 | 14.4/8.4/3.3 | 480/57 | (0.138, 0.273) |
| DtPAPy (1wt%) TSF-Device | 3.3 | 4512 | 22.4/14.3/6.0 | 21.4/7.0/1.8 | 12.0/7.8/3.3 | 480/57 | (0.140, 0.290) |
| DtPAPy (3wt%) TSF-Device | 3.3 | 4794 | 16.3/10.7/5.4 | 15.7/5.4/1.6 | 8.2/5.5/2.8 | 484/55 | (0.143, 0.322) |

[a)] Voltage at 1 cd $m^{-2}$ (V); [b)] Maximum luminance (cd $m^{-2}$); Current efficiency (cd $A^{-1}$): maximum, values at 100 cd $m^{-2}$, 1000 cd $m^{-2}$; Power efficiency (lm $W^{-1}$): maximum, values at 100 cd $m^{-2}$, 1000 cd $m^{-2}$; External quantum efficiency (%): maximum, values at 100 cd $m^{-2}$, 1000 cd $m^{-2}$; [c)] The peak of the EL spectrum; Full width at half maximum of EL spectrum; [d)] Commission Internationale de l'Eclairage coordinates.

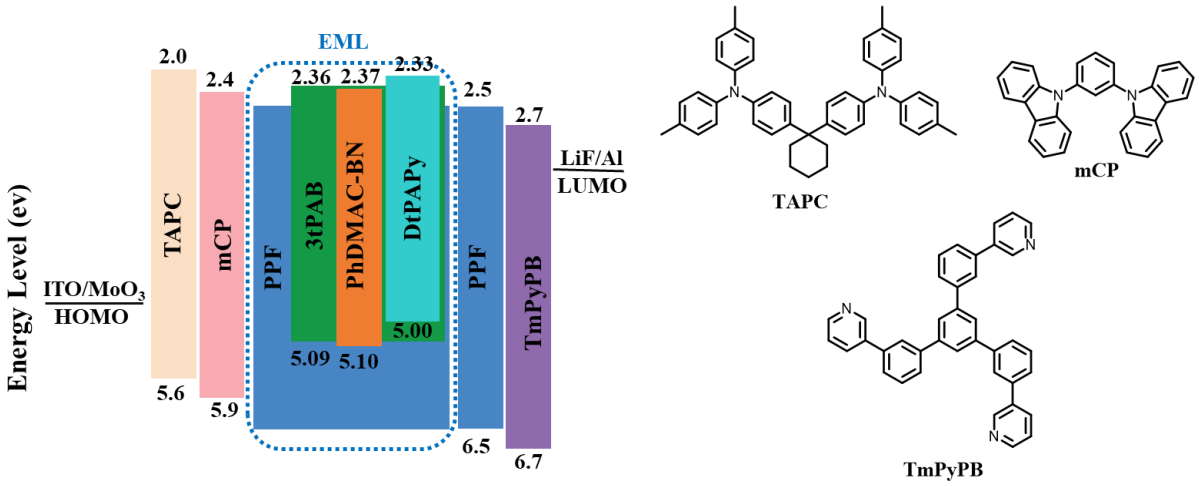


**Figure S9.** Device configuration and the energy level diagrams of TSF device and TST device.

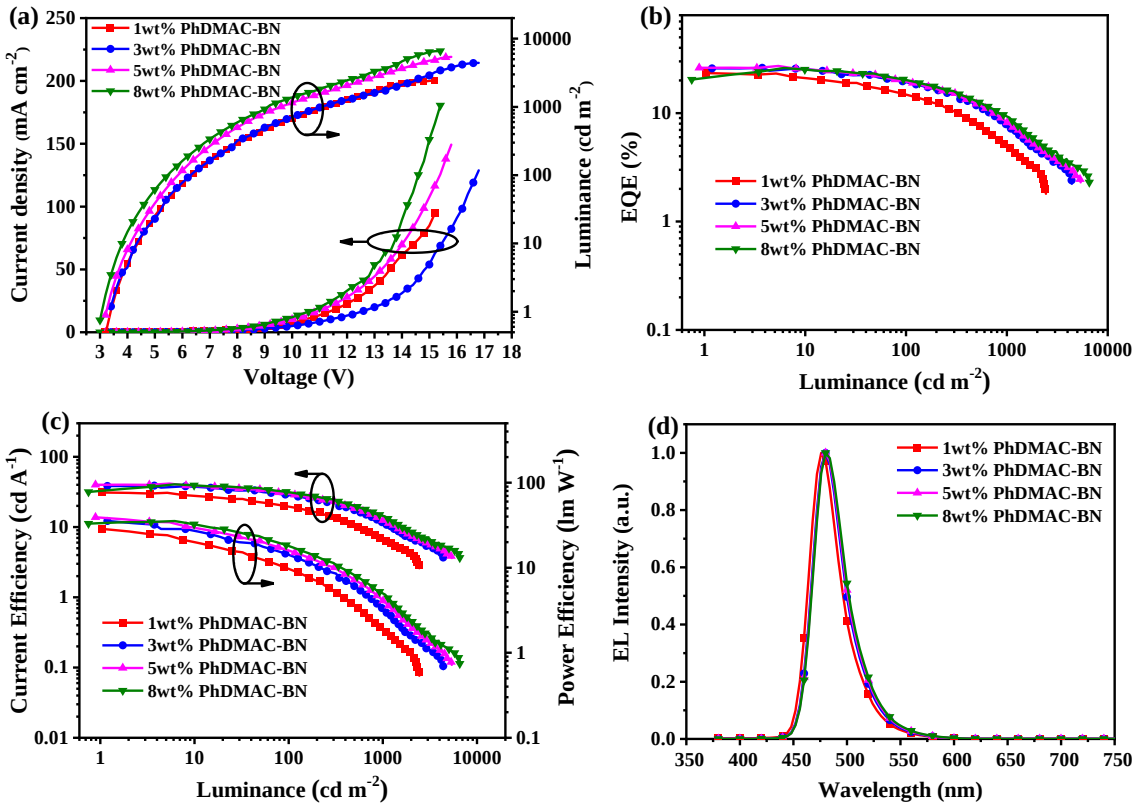


**Figure S10.** EL characteristics of PhDMAC-BN in simple doped OLEDs with structures of ITO/ $MoO_3$ (10 nm)/ TAPC (60 nm)/ mCP (10 nm)/ PPF: x wt% PhDMAC-BN (20 nm, x=1, 3, 5, 8)/ PPF (10 nm)/ TmPyPB (30 nm)/ LiF (1 nm)/ Al (100 nm). a) Current density-voltage-brightness (J-V-B) characteristics. b) EQE-brightness curves. c) current efficiency-brightness-power efficiency curves. d) normalized EL spectra at 6 V.

**Table S5** The EL performances of PhDMAC-BN in simple doped OLEDs

| Compound | $V_{on}$[a] (V) | $L_{max}$[b] (cd $m^{-2}$) | $CE_{max}$[b] (cd $A^{-1}$) | $PE_{max}$[b](lm $W^{-1}$) | $EQE_{max}$[b] (%) | $\lambda_{EL}$[c] /FWHM[c] (nm) | CIE[d] (x, y) |
|---|---|---|---|---|---|---|---|
| PhDMAC-BN (1wt%) | 3.4 | 2446 | 31.0/19.2/6.7 | 28.7/9.4/1.9 | 23.4/14.6/4.9 | 476/34 | (0.111, 0.208) |
| PhDMAC-BN (3wt%) | 3.4 | 4414 | 38.9/28.0/11.2 | 35.5/13.7/3.1 | 26.2/18.9/7.5 | 480/34 | (0.105, 0.253) |
| PhDMAC-BN (5wt%) | 3.2 | 5398 | 41.5/29.9/12.5 | 39.2/16.2/4.1 | 27.2/19.7/8.2 | 480/34 | (0.105, 0.264) |
| PhDMAC-BN (8wt%) | 3.1 | 6578 | 40.6/31.8/14.1 | 35.4/18.5/4.8 | 26.1/20.5/9.1 | 480/35 | (0.105, 0.272) |

[a)] Voltage at 1 cd $m^{-2}$ (V); [b)] Maximum luminance (cd $m^{-2}$); Current efficiency (cd $A^{-1}$): maximum, values at 100 cd $m^{-2}$, 1000 cd $m^{-2}$; Power efficiency (lm $W^{-1}$): maximum, values at 100 cd $m^{-2}$, 1000 cd $m^{-2}$; External quantum efficiency (%): maximum, values at 100 cd $m^{-2}$, 1000 cd $m^{-2}$; [c)] The peak of the EL spectrum; Full width at half maximum of EL spectrum; [d)] Commission Internationale de l'Eclairage coordinates.

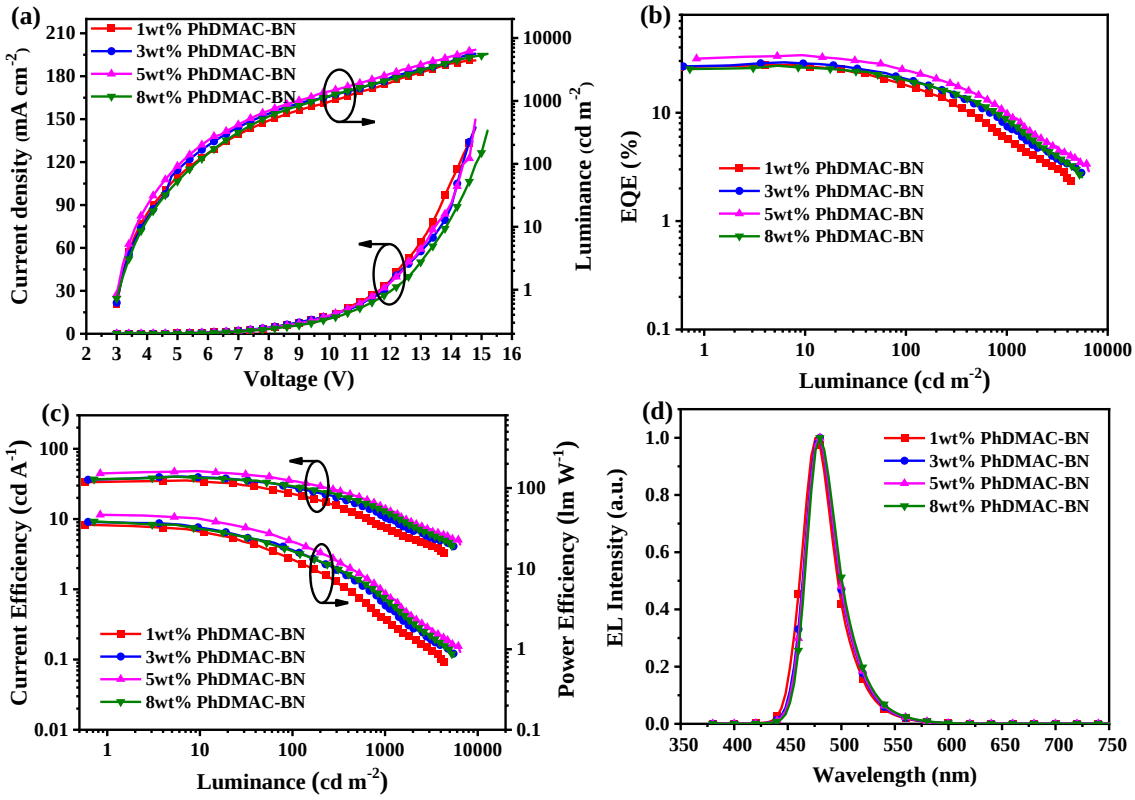


**Figure S11.** EL characteristics of PhDMAC-BN in TST device with structures of ITO/ MoO3 (10 nm)/ TAPC (60 nm)/ mCP (10 nm)/ PPF: 20 wt% 3tPAB: x wt% PhDMAC-BN (20 nm, x=1, 3, 5, 8)/ PPF (10 nm)/ TmPyPB (30 nm)/ LiF (1 nm)/ Al (100 nm). a) Current density-voltage-brightness (J-V-B) characteristics. b) EQE-brightness curves. c) current efficiency-brightness-power efficiency curves. d)

normalized EL spectra at 6 V.

**Table S6.** The EL performances of PhDMAC-BN in TST device

| Compound | $V_{on}$[a] (V) | $L_{max}$[b] (cd $m^{-2}$) | $CE_{max}$[b] (cd $A^{-1}$) | $PE_{max}$[b](lm $W^{-1}$) | $EQE_{max}$[b] (%) | $\lambda_{EL}$[c] /FWHM[c] (nm) | CIE[d] (x, y) |
|---|---|---|---|---|---|---|---|
| PhDMAC-BN (1wt%) | 3.1 | 4395 | 35.4/22.4/8.0 | 35.0/12.6/2.5 | 27.8/17.6/6.1 | 476/35 | (0.113, 0.193) |
| PhDMAC-BN (3wt%) | 3.1 | 5616 | 40.3/28.4/10.4 | 38.0/17.2/3.5 | 29.2/20.6/7.5 | 480/35 | (0.108, 0.223) |
| PhDMAC-BN (5wt%) | 3.1 | 6491 | 48.1/35.5/13.9 | 46.6/22.3/4.8 | 33.9/25.1/9.7 | 480/35 | (0.108, 0.223) |
| PhDMAC-BN (8wt%) | 3.1 | 5589 | 40.2/29.4/13.1 | 38.6/16.5/4.4 | 27.1/19.9/8.8 | 480/35 | (0.106, 0.250) |

[a)] Voltage at 1 cd $m^{-2}$ (V); [b)] Maximum luminance (cd $m^{-2}$); Current efficiency (cd $A^{-1}$): maximum, values at 100 cd $m^{-2}$, 1000 cd $m^{-2}$; Power efficiency (lm $W^{-1}$): maximum, values at 100 cd $m^{-2}$, 1000 cd $m^{-2}$; External quantum efficiency (%): maximum, values at 100 cd $m^{-2}$, 1000 cd $m^{-2}$; [c)] The peak of the EL spectrum; Full width at half maximum of EL spectrum; [d)] Commission Internationale de l'Eclairage coordinates.

**Table S7.** PL characteristics and rate constants of PPF: 20 wt% 3tPAB, PPF: 20 wt% 3tPAB: 0.5 wt% DtPAPy and PPF: 20 wt% 3tPAB: 5 wt% PhDMAC-BN films.

| Compound | $\lambda_{em}$ | PLQY (%) | $\tau_{PF}$[a] (ns) | $\tau_{DF}$[a] (μs) | $k_{RISC}$[b] ($\times 10^4$ $s^{-1}$) | $k_{FET}$[c] ($\times 10^7$ $s^{-1}$) |
|---|---|---|---|---|---|---|
| 3tPAB | 459 | 0.783 | 9.7 | 59.0 | 2.39 | - |
| 3tPAB：DtPAPy | 483 | 0.828 | 5.7 | 11.0 | 2.39 | 7.23 |
| 3tPAB: PhDMAC-BN | 482 | 0.970 | 5.4 | 17.4 | 2.39 | 8.21 |

[a)] $k_{PF} = 1/\tau_{PF}$, $k_{PF} = 1/\tau_{PF}$; [b)] reverse intersystem crossing rate constant of sensitizer; [c)] $k_{FET} = 1/\tau_{PF,\ x\ wt\%} - 1/\tau_{PF,\ 0\ wt\%}$

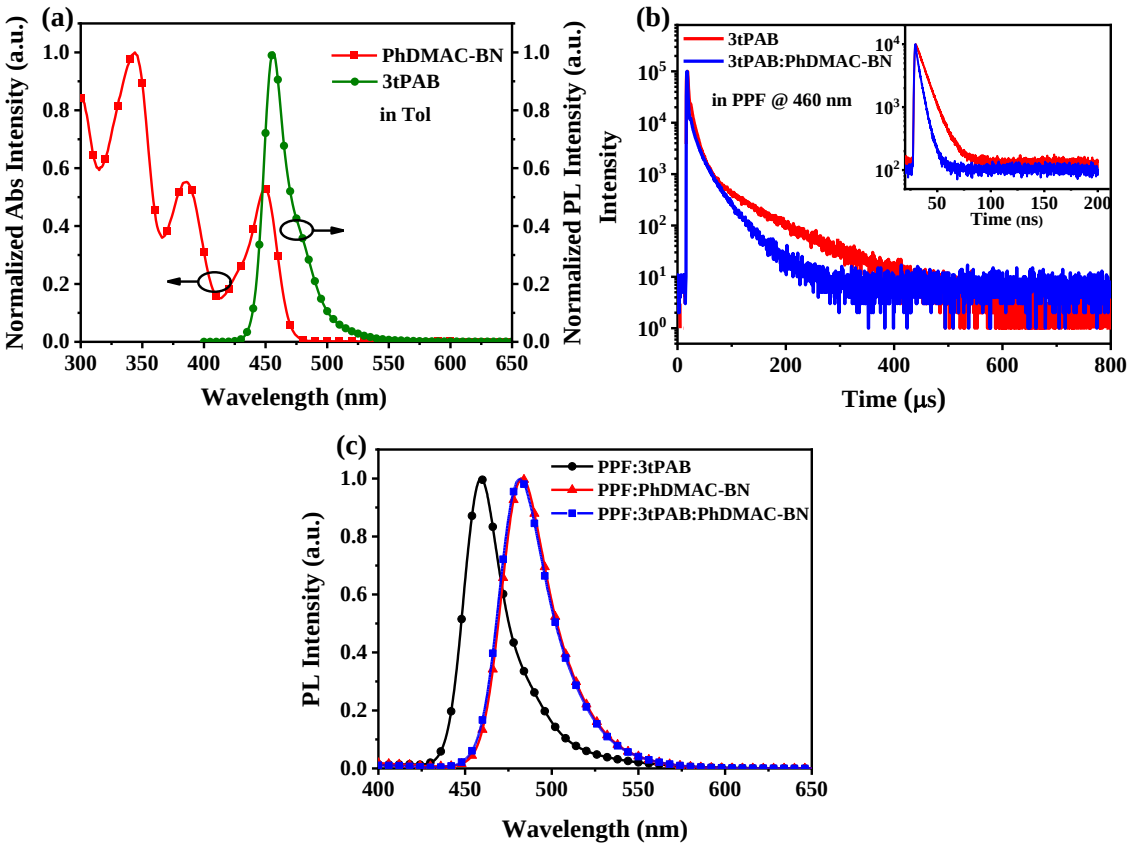


**Figure S12.** a) The absorption spectra of PhDAMC-BN, and PL spectra of 3tPAB in toluene ($1.0 \times 10^{-5}$ M). b) The transient PL spectra of PPF: 20wt% 3tPAB and PPF: 20wt% 3tPAB: 5wt% PhDAMC-BN films, which was observed at 460 nm. c) PL spectra for PPF: 20 wt% 3tPAB, PPF: 5 wt% PhDMAC-BN, and PPF: 20wt% 3tPAB: 5 wt% PhDMAC-BN films.

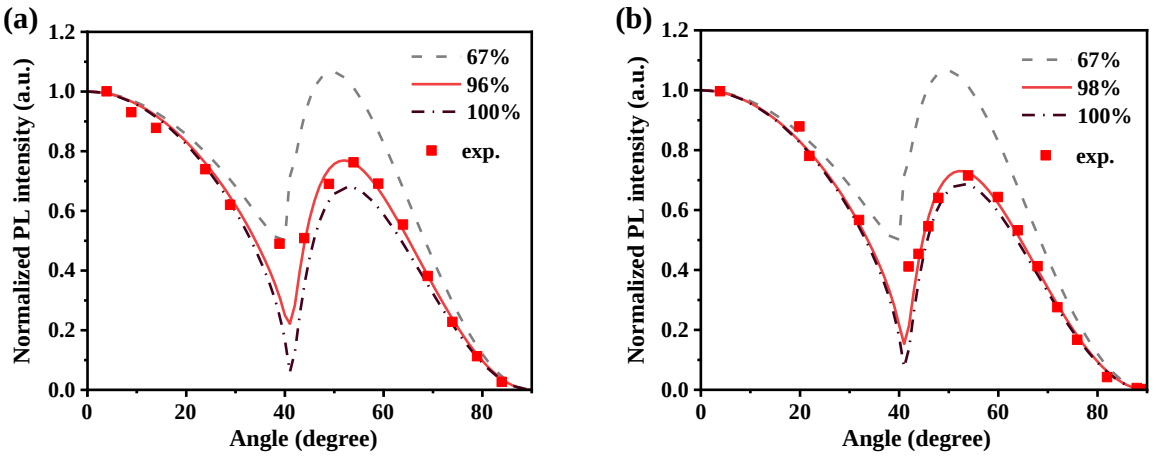


**Figure S13.** Angle-dependent *p*-polarized PL intensity and simulation curve for a) PPF: 5 wt% PhDMAC-BN and b) PPF: 20wt% 3tPAB: 5 wt% PhDMAC-BN films.

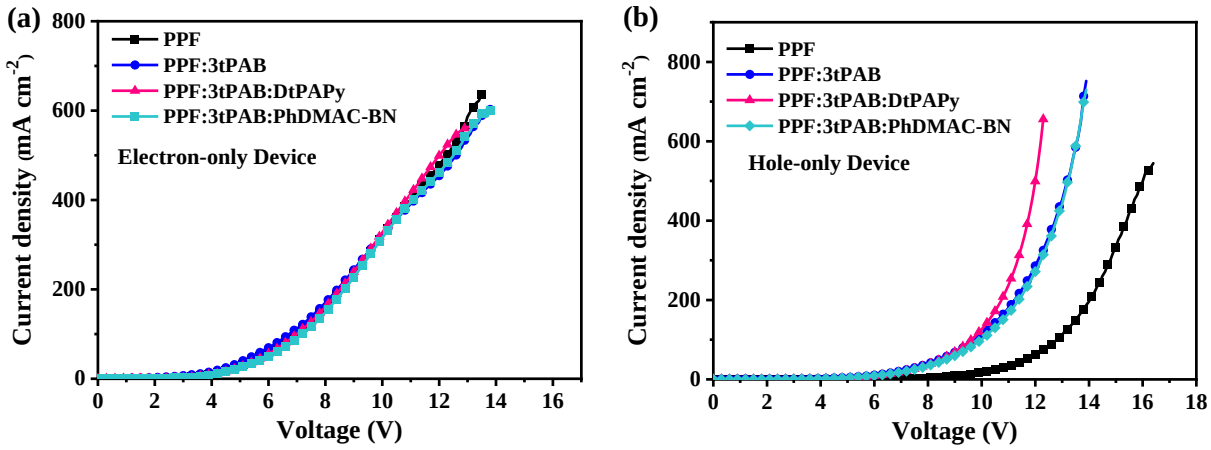


**Figure S14**. Current density-voltage (J-V) curves of electron-only (a) and hole-only (b) devices for PPF host only, 20wt% 3tPAB in PPF host, 20wt% 3tPAB: 0.5wt% DtPAPy in PPF host, and 20wt% 3tPAB: 5wt% PhDMAC-BN in PPF host.

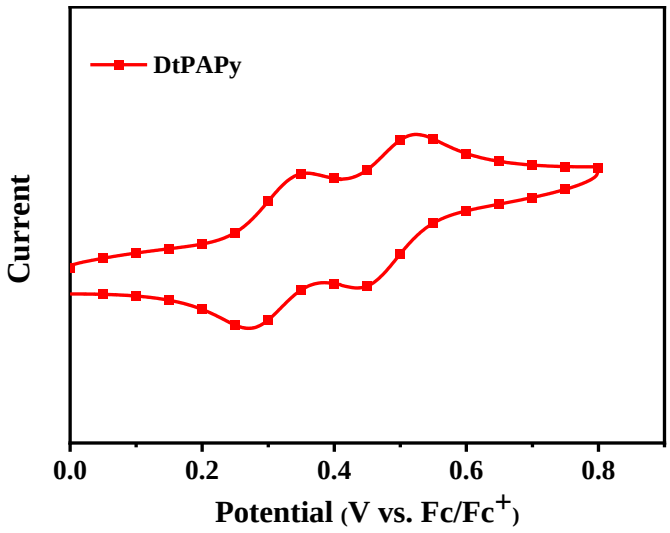


**Figure S15.** Cyclic voltammogram of DtPAPy.

**Table S8** The device performance of published blue fluorescence and MR-TADF OLEDs using TADF emitter as sensitizer.

| TADF sensitizer | dopant | $V_{on}$[a] (V) | $CE_{max}$[b] (cd $A^{-1}$) | $PE_{max}$[b](lm $W^{-1}$) | $EQE_{max}$[b] (%) | $\lambda_{EL}$[c] /FWHM[c] (nm) | CIE[d] (x, y) | Ref. |
|---|---|---|---|---|---|---|---|---|
| ACRSA | TBPe | 4.7 | 27 | 18 | 13.4 | -/- | (0.17, 0.30) | [2] |
| CzAcSF | TBPe | 4.2 | 29.8 | 31.2 | 18.1 | -/- | (0.15, 0.22) | [3] |
| DMAC-DMT | BPPyA | - | 18.3 | - | 19.0 | -/- | (0.14, 0.15) | [4] |
| DMAC-DPS | t-DABNA | - | 32.6 | 33.6 | 31.4 | -/31 | (0.13, 0.15) | [5] |
| 5Cz-TRZ | TBPe | - | - | - | 24.0 | -/- | - | [6] |

| | | | | | | | | |
|---|---|---|---|---|---|---|---|---|
| TpAT-tFFO | TBPe | - | - | - | 18.7 | -/- | (0.15, 0.23) | [7] |
| p4TCzPhBN | t-DABNA | - | - | - | 32.5 | -/- | (0.13, 0.12) | [8] |
| DBA–BFICz | *v*-DABNA | 3.1 | 30.0 | - | 38.8 | 473/19 | (0.12, 0.15) | [9] |
| DBA–BTICz | *v*-DABNA | 3.1 | 28.3 | - | 37.3 | 473/19 | (0.12, 0.15) | |
| HDT-1 | *v*-DABNA | 3.0 | 39 | 41 | 27 | 470/18 | (0.15, 0.20) | [10] |
| PPCzTrz | *v*-DABNA | - | 30.3 | - | 33.2 | 473/- | (0.13, 0.14) | [11] |
| PCzTrz | *v*-DABNA | - | 35.5 | - | 33.5 | 473/ | (0.12, 0.18) | |
| TPh2Cz2DPhCzBN | CzBNCz | 3.2 | 42.6 | 47.8 | 21.9 | 471/50 | (0.160, 0.305) | [12] |
| TPh2Cz2DPhCzBN | DABNA2 | 3.6 | 46.3 | 45.4 | 24.1 | 471/61 | (0.158, 0298) | |
| pMDBA-DI | t-Bu-*v*-DABNA. | 2.9 | 37.9 | - | 36.2 | 474/19 | (0.13, 0.19) | [13] |
| mMDBA-DI | t-Bu-*v*-DABNA | 2.9 | 30.3 | - | 39.1 | 474/19 | (0.12, 0.15) | |
| DPAc-DtCzBN | pICz | 3.5 | 30.1 | 25.4 | 32.0 | 445/41 | (0.15, 0.10) | [14] |
| DPAc-DtCzBN | pICz-TPA | 3.6 | 31.5 | 27.1 | 34.7 | 445/30 | (0.15, 0.085) | |
| CTPCF3 | DtBuCzB | 3.0 | - | - | 27.5 | 488/29 | (0.13,0.40) | [15] |
| CTPCF3 | S-Cz-BN | 3.0 | - | - | 30.5 | 488/26 | (0.12,0.43) | |
| CTPCF3 | D-Cz-BN | 3.0 | - | - | 36.3 | 488/24 | (0.11,0.43) | |
| USF | PTZBN1 | 2.8 | 73.3 | 82.2 | 32.7 | 489/47 | (0.14, 0.41) | [16] |
| USF | PTZBN2 | 2.8 | 67.4 | 75.6 | 34.8 | 478/48 | (0.15, 0.29) | |
| USF | PTZBN3 | 2.8 | 55.7 | 62.5 | 32.0 | 468/46 | (0.15, 0.24) | |
| HDT-1 | CzBN | 3.3 | 48.7 | 38.2 | 22.0 | 478/39 | (0.142, 0.287) | [17] |
| HDT-1 | CzBNNa | 2.9 | 41.8 | 50.5 | 20.5 | 484/42 | (0.149, 0.360) | |
| HDT-1 | CzBNPyr | 3.2 | 41.5 | 37.1 | 19.4 | 483/34 | (0.133, 0.318) | |
| 3Cz2BN | BN1 | 4.3 | 20.9 | 14.9 | 31.2 | 457/28 | (0.14, 0.08) | [18] |
| 3Cz2BN | BN2 | 4.3 | 29.7 | 20.3 | 33.2 | 467/23 | (0.13, 0.11) | |
| 3Cz2BN | BN3 | 4.1 | 27.5 | 19.0 | 37.6 | 458/23 | (0.14, 0.08) | |
| 4PhCz2BN | *v*-DABNA | 3.2 | 25.4 | 25.0 | 22.4 | 470/18 | (0.13,0.15) | [19] |
| 4TCzBN | m[B-N]N1 | 2.6 | 58.6 | 61.9 | 36.0 | 479/27 | (0.115, 0.272) | [20] |
| 4TCzBN | m[B-N]N2 | 2.6 | 48.4 | 53.5 | 33.4 | 485/33 | (0.112, 0.319) | |
| m4TCzPhBN | pSFIAc1 | 3.4 | - | 14.9 | 24.9 | 446/21 | (0.148, 0.058) | [21] |
| m4TCzPhBN | pSFIAc2 | 3.5 | - | 23.0 | 31.4 | 451/21 | (0.146, 0.078) | |
| DtBuAc-DBT | α-3BNMes | 3.4 | - | - | 14.6 | 443/49 | (0.15, 0.10) | [22] |
| 4TCzPhBN | BIC-mCz | 3.3 | - | 9.7 | 19.4 | 432/42 | (0.16, 0.05) | [23] |
| 4TCzPhBN | mDBIC | 3.4 | - | 9.7 | 13.5 | 431/42 | (0.16, 0.05) | |
| p4TCzPhBN | BIC-pCz | 3.0 | - | 51.1 | 39.8 | 466/48 | (0.14, 0.16) | |
| 23PCX | *v*-DABNA | - | - | 40.4 | 25.1 | 471/24 | (0.149, 0.241) | [24] |
| 33PCX | *v*-DABNA | - | - | 24.1 | 20.6 | 471/21 | (0.140, 0.195) | |
| **3tPAB** | PhDMAC-BN | 3.1 | 48.1 | 46.6 | 33.9 | 480/35 | (0.108, 0.223) | **This work** |

[a] Voltage at 1 cd $m^{-1}$ (V). [b] Maximum luminance (cd $m^{-1}$); Maximum current efficiency (cd $A^{-1}$); Maximum power efficiency (lm $W^{-1}$); Maximum external quantum efficiency (%). [c] The peak of the EL spectrum; Full width at half maximum of EL spectrum. [d] Commission Internationale de l'Eclairage coordinates.

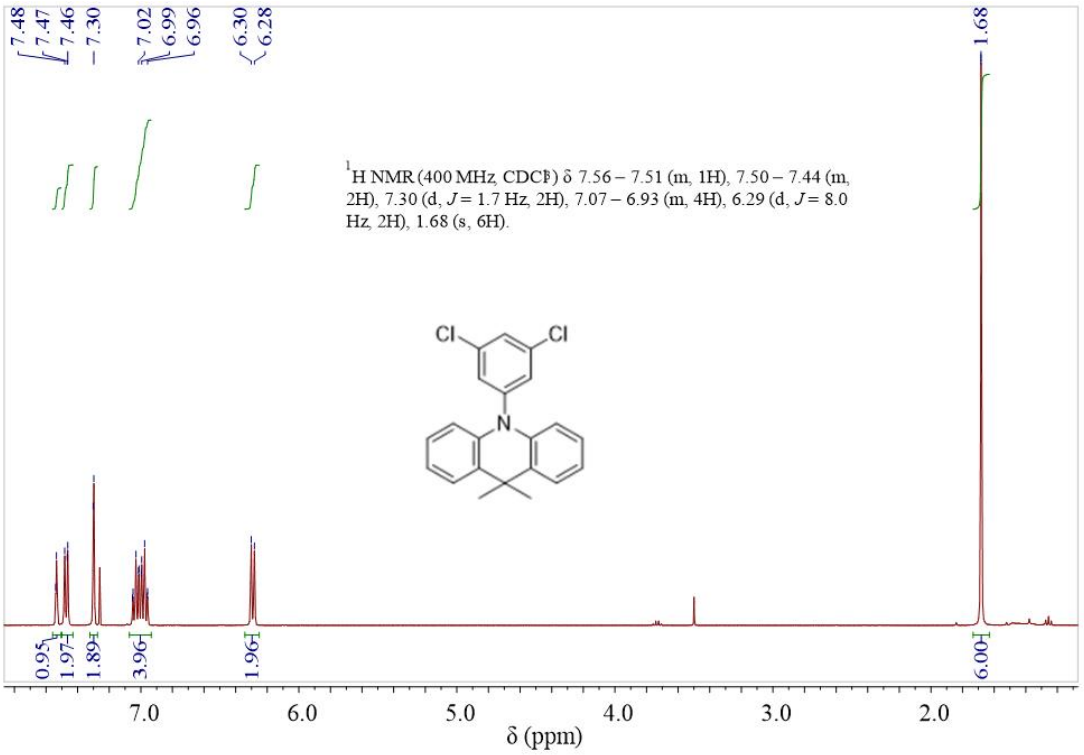


**Figure S16.** $^1$H NMR spectrum of 1 in $CDCl_3$.

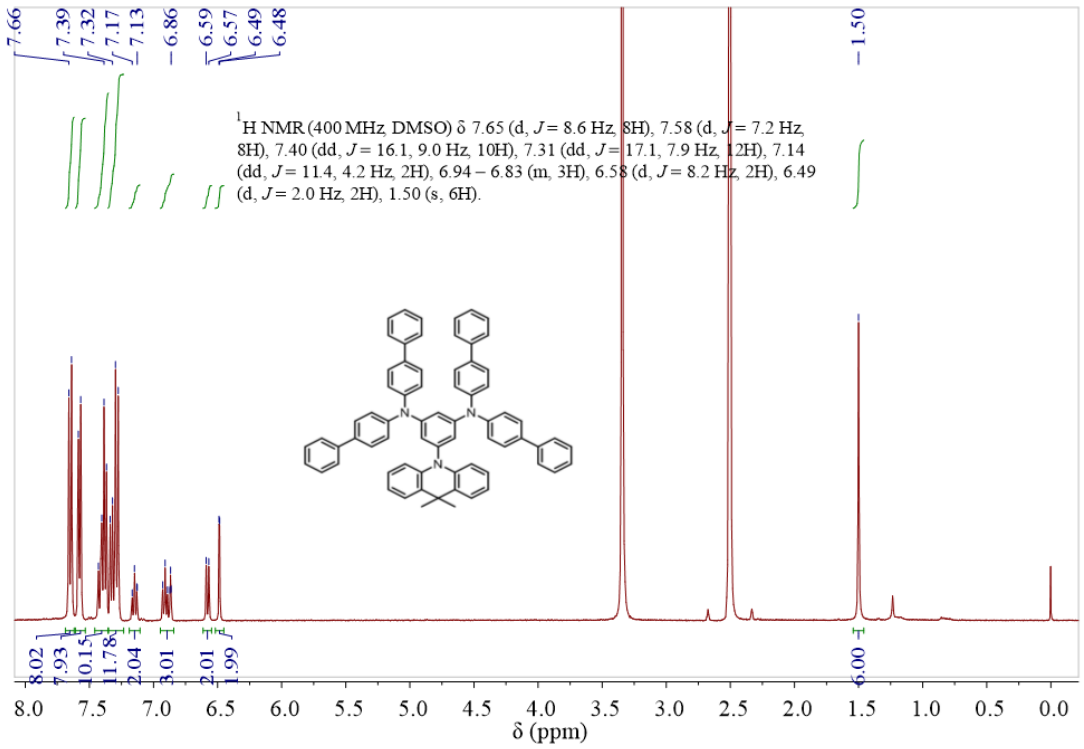


**Figure S17.** $^1$H NMR spectrum of 2 in DMSO.

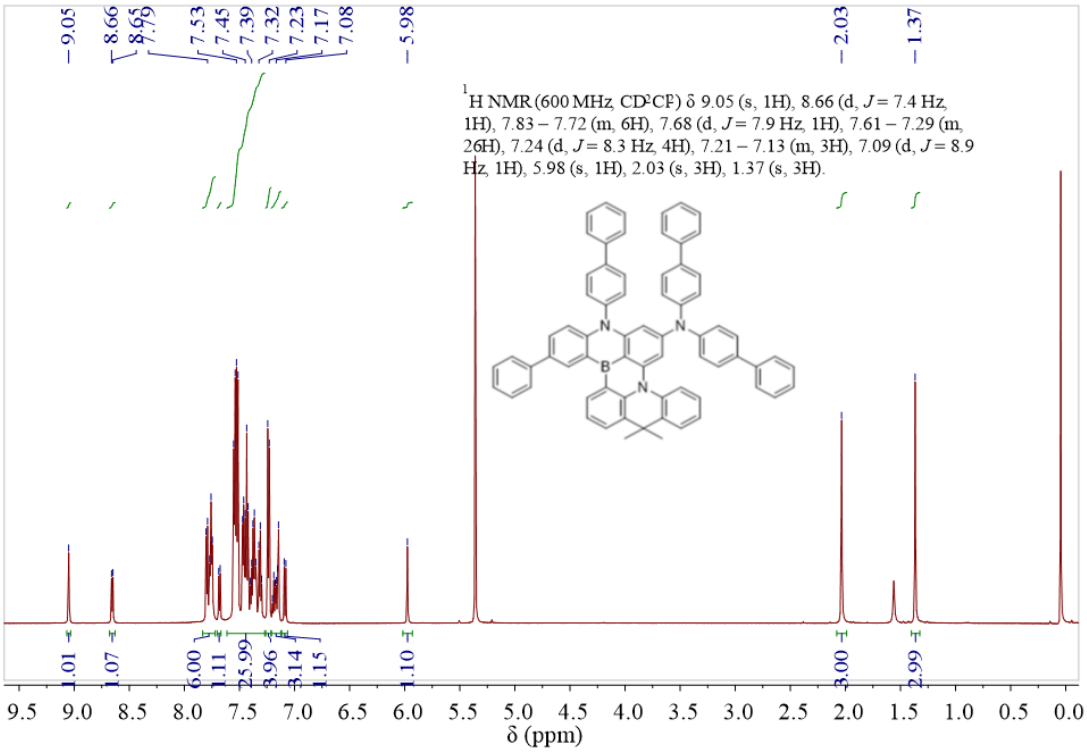


**Figure S18.** $^{1}$H NMR spectrum of PhDMAC-BN in $CD_2Cl_2$.

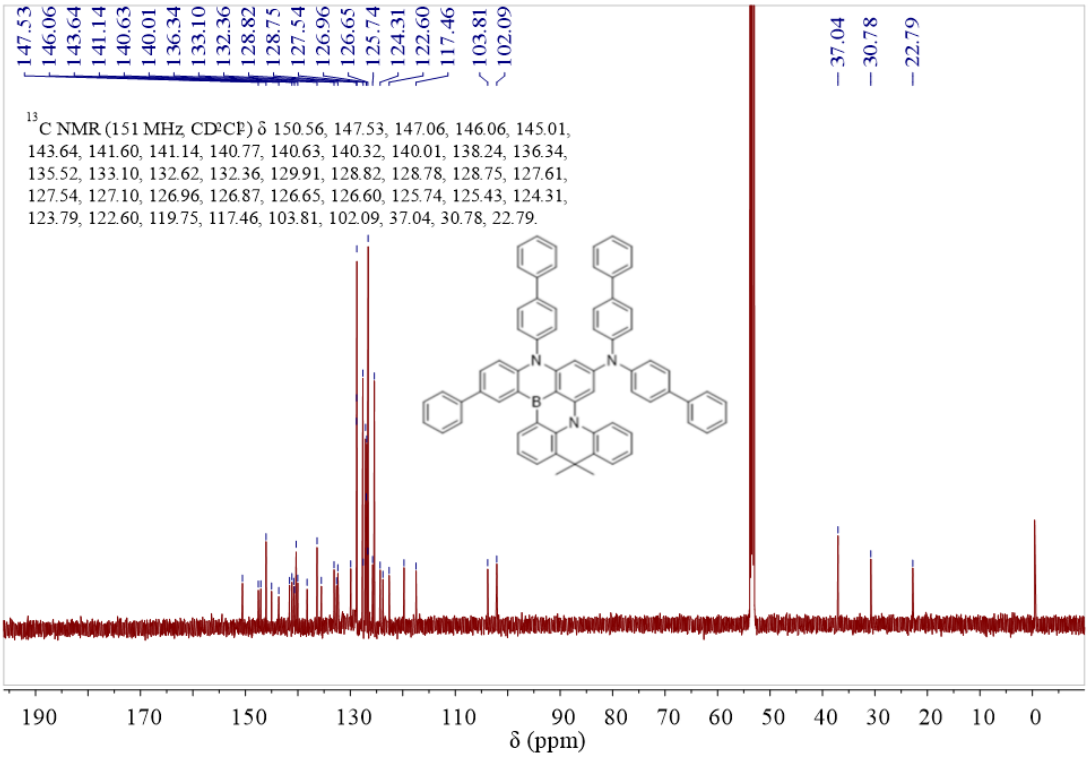


**Figure S19.** $^{13}$C NMR spectrum of PhDMAC-BN in $CD_2Cl_2$.

**References**


[1] a) Q. Zhang, H. Kuwabara, J. William J. Potscavage, S. Huang, Y. Hatae, T. Shibata, C. Adachi, *J. Am. Chem. Soc.* **2014**, 136, 18070; b) Q. Zhang, B. Li, S. Huang, H. Nomura, H. Tanaka, C. Adachi, *Nat. Photon.* **2014**, 8, 326; c) H. Kaji, H. Suzuki, T. Fukushima, K. Shizu, K. Suzuki, S. Kubo, T. Komino, H. Oiwa, F. Suzuki, A. Wakamiya, Y. Murata, C. Adachi, *Nat. Commun.* **2015**, 6, 8476.

[2] H. Nakanotani, T. Higuchi, T. Furukawa, K. Masui, K. Morimoto, M. Numata, H. Tanaka, Y. Sagara, T. Yasuda, C. Adachi, *Nat. Commun.* **2014**, 5, 4016.

[3] I. H. Lee, W. Song, J. Y. Lee, S.-H. Hwang, *J. Mater. Chem. C* **2015**, 3, 8834.

[4] D. H. Ahn, J. H. Jeong, J. Song, J. Y. Lee, J. H. Kwon, *ACS Appl. Mater. Interfaces* **2018**, 10, 10246.

[5] S. H. Han, J. H. Jeong, J. W. Yoo, J. Y. Lee, *J. Mater. Chem. C* **2019**, 7, 3082.

[6] L.-S. Cui, A. J. Gillett, S.-F. Zhang, H. Ye, Y. Liu, X.-K. Chen, Z.-S. Lin, E. W. Evans, W. K. Myers, T. K. Ronson, H. Nakanotani, S. Reineke, J.-L. Bredas, C. Adachi, R. H. Friend, *Nat. Photon.* **2020**, 14, 636.

[7] Y. Wada, H. Nakagawa, S. Matsumoto, Y. Wakisaka, H. Kaji, *Nat. Photon.* **2020**, 14, 643.

[8] D. Zhang, X. Song, A. J. Gillett, B. H. Drummond, S. T. E. Jones, G. Li, H. He, M. Cai, D. Credgington, L. Duan, *Adv. Mater.* **2020**, 32, 1908355.

[9] R. Braveenth, H. Lee, J. D. Park, K. J. Yang, S. J. Hwang, K. R. Naveen, R. Lampande, J. H. Kwon, *Adv. Funct. Mater.* **2021**, 31, 2105805.

[10] C.-Y. Chan, M. Tanaka, Y.-T. Lee, Y.-W. Wong, H. Nakanotani, T. Hatakeyama, C. Adachi, *Nat. Photon.* **2021**, 15, 203.

[11] S. O. Jeon, K. H. Lee, J. S. Kim, S.-G. Ihn, J. W. Kim, H. Lee, S. Kim, H. Choi, J. Y. Lee, Y. S. Chung, *Nat. Photon.* **2021**, 15, 208.

[12] Y. T. Lee, C. Y. Chan, M. Tanaka, M. Mamada, U. Balijapalli, Y. Tsuchiya, H. Nakanotani, T. Hatakeyama, C. Adachi, *Adv. Electron. Mater.* **2021**, 7, 2001090.

[13] K. R. Naveen, H. Lee, R. Braveenth, D. Karthik, K. J. Yang, S. J. Hwang, J. H.

Kwon, *Adv. Funct. Mater.* **2022**, 32, 2110356.

[14] J. Wei, C. Zhang, D. Zhang, Y. Zhang, Z. Liu, Z. Li, G. Yu, L. Duan, *Angew. Chem. Int. Ed.* **2021**, 60, 12269.

[15] Y. Zhang, J. Wei, D. Zhang, C. Yin, G. Li, Z. Liu, X. Jia, J. Qiao, L. Duan, *Angew. Chem. Int. Ed.* **2022**, 61, e202113206.

[16] T. Hua, J. Miao, H. Xia, Z. Huang, X. Cao, N. Li, C. Yang, *Adv. Funct. Mater.* **2022**, 32, 2201032.

[17] Y. T. Lee, C. Y. Chan, M. Tanaka, M. Mamada, K. Goushi, X. Tang, Y. Tsuchiya, H. Nakanotani, C. Adachi, *Adv. Opt. Mater.* **2022**, DOI: 10.1002/adom.202200682.

[18] X. Lv, J. Miao, M. Liu, Q. Peng, C. Zhong, Y. Hu, X. Cao, H. Wu, Y. Yang, C. Zhou, J. Ma, Y. Zou, C. Yang, *Angew. Chem. Int. Ed.* **2022**, 61, e202201588.

[19] M. Mamada, H. Katagiri, C. Y. Chan, Y. T. Lee, K. Goushi, H. Nakanotani, T. Hatakeyama, C. Adachi, *Adv. Funct. Mater.* **2022**, 32, 2204352.

[20] G. Meng, H. Dai, T. Huang, J. Wei, J. Zhou, X. Li, X. Wang, X. Hong, C. Yin, X. Zeng, Y. Zhang, D. Yang, D. Ma, G. Li, D. Zhang, L. Duan, *Angew. Chem. Int. Ed.* **2022**, DOI: 10.1002/anie.202207293.

[21] G. Meng, D. Zhang, J. Wei, Y. Zhang, T. Huang, Z. Liu, C. Yin, X. Hong, X. Wang, X. Zeng, D. Yang, D. Ma, G. Li, L. Duan, *Chem. Sci.* **2022**, 13, 5622.

[22] K. Stavrou, S. Madayanad Suresh, D. Hall, A. Danos, N. A. Kukhta, A. M. Z. Slawin, S. Warriner, D. Beljonne, Y. Olivier, A. Monkman, E. Zysman-Colman, *Adv. Opt. Mater.* **2022**, DOI: 10.1002/adom.202200688.

[23] X. Wang, Y. Zhang, H. Dai, G. Li, M. Liu, G. Meng, X. Zeng, T. Huang, L. Wang, Q. Peng, D. Yang, D. Ma, D. Zhang, L. Duan, *Angew. Chem. Int. Ed.* **2022**, DOI: 10.1002/anie.202206916.

[24] D. Zhang, Y. Wada, Q. Wang, H. Dai, T. Fan, G. Meng, J. Wei, Y. Zhang, K. Suzuki, G. Li, L. Duan, H. Kaji, *Adv. Sci.* **2022**, 9, 2106018.